
Causal Temporal Regime Structure Learning

Abdellah Rahmani
LTS4, EPFL, Switzerland
abdellah.rahmani@epfl.ch

Pascal Frossard
LTS4, EPFL, Switzerland
pascal.frossard@epfl.ch

Abstract

We address the challenge of structure learning from multivariate time series that are characterized by a sequence of different, unknown regimes. We introduce a new optimization-based method (CASTOR), that concurrently learns the Directed Acyclic Graph (DAG) for each regime and determine the number of regimes along with their sequential arrangement. Through the optimization of a score function via an expectation maximization (EM) algorithm, CASTOR alternates between learning the regime indices (Expectation step) and inferring causal relationships in each regime (Maximization step). We further prove the identifiability of regimes and DAGs within the CASTOR framework. We conduct extensive experiments and show that our method consistently outperforms causal discovery models across various settings (linear and nonlinear causal relationships) and datasets (synthetic and real data).

1 Introduction

Uncovering the causal relationships among Multivariate Time Series (MTS) variables and understanding how they evolve over time is crucial in numerous fields, because causal structures help to understand the complex mechanisms in the real world, like diseases [38] or earth systems [35]. A multitude of causal discovery approaches focus on extracting causality from observational data sources [7, 12, 22, 24, 25, 27, 33, 43]. Various research works, such as those introducing models like DYNOTEARS [27] and Rhino [12], have aimed to address many challenges, including inferring both linear and nonlinear causal relationships and managing instantaneous as well as time-lagged connections. Nevertheless, a prevalent assumption in many existing methods is that time series observations originate from a single "domain/regime" governed by one causal graph. This assumption is often inadequate in real-world scenarios, such as climate science where causal dependencies are regime dependent (warm and cold regimes [19]) and Electroencephalographic (EEG) time series in epilepsy settings [32, 41] where recordings exhibit several unknown regimes (non-seizure, pre-seizure, and seizure) for example. Often successive regimes actually originate from different causal models on the same set of variables, each one is described by a different temporal causal graph.

CD-NOD [16], tackles MTS with various regimes. By using the time stamp IDs as a surrogate variable, CD-NOD output one summary causal graph where the parents of each variable are identified as the union of all its parents in graphs from different regimes. Then it detects the change points by using a non stationary driving force that estimates the variability of the conditional distribution $p(x_i | \text{union parents of } x_i)$ over the time index surrogate. While CD-NOD provides a summary graph, it falls short in inferring individual causal graphs. The summary graph fails to emphasize the edges that vanish or emerge during the shift from one regime to another. Additionally, CD-NOD detects the change points but fails to determine the regime indices, rendering it incapable of inferring the precise number of regimes. In scenarios involving recurring regimes, CD-NOD is unable to detect this crucial information. Another relevant work dealing with MTS composed of multiple regimes is RPCMCI [37] which learns a temporal graph for each regime. However, it focuses initially on inferring only time-lagged relationships and requires prior knowledge of the number of regimes

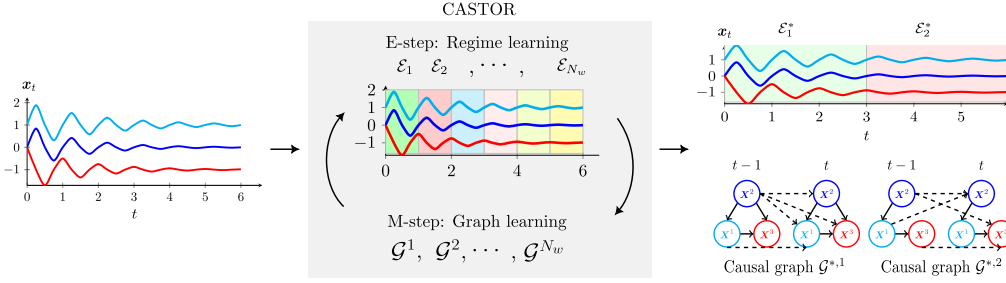


Figure 1: The illustration demonstrates that CASTOR takes a MTS as input and uses a EM procedure to infer the number of regimes (equal to 2), the regime partition (\mathcal{E}_1^* for the first regime and \mathcal{E}_2^* for the second) and learn the temporal causal graphs. Dashed edges symbolize time-lagged links, while normal arrows represent instantaneous links.

and transitions between them. Overall, the above methods make certain assumptions that may limit their applicability in practical settings.

We introduce CASTOR (Figure 1), at the best of our knowledge the first framework designed to learn linear and nonlinear temporal causal relationships from MTS composed of multiple regimes (each regime corresponds to a MTS block), without necessitating prior knowledge of regime indices and the total number of regimes. CASTOR maximizes a score function via Expectation Maximization (EM) algorithm to infer the number of regimes, their indices and learn the DAG for each regime. We further prove the identifiability of regimes and graphs within the CASTOR framework (identifiability of regimes and causal graphs for MTS with multiple regimes). We conduct an extensive comparative analysis between CASTOR and specialized causal discovery models designed for MTS composed of multiple successive regimes, namely RPCMCI [37] and CD-NOD [16]. Our findings demonstrate the superior performance of CASTOR across various scenarios. Additionally, we compare CASTOR with models like DYNOTEARS [27], Rhino [12] and PCMCI+ [34] tailored for MTS characterized by a single regime. Even when we provide these baselines with the true regime partition information, our approach consistently outperforms them in inferring the DAGs on both synthetic data and real-world datasets. We finally apply CASTOR to real-world Biosphere-Atmosphere data where the results show its ability to detect meaningful regimes and also generate explanatory DAGs.

2 Framework

In this section, we introduce the various notations used in our paper, define the temporal causal graph, describe the setting of multivariate time series (MTS) with multiple regimes, and present a new Structural Equation Model (SEM) for these MTS.

Notation. We denote a temporal causal graph (definition 2.1) by $\mathcal{G} = (\mathbf{V}, E)$, it is represented by a collection of adjacency matrices, collectively denoted as $\mathcal{G}_{\tau \in [0:L]} = \{\mathcal{G}_0, \dots, \mathcal{G}_L\}$. Matrices, vectors and scalars are denoted by uppercase bold (\mathcal{G}_τ), lowercase bold (\mathbf{x}_t) and lowercase normal letters ($x_{t-\tau}^i$), respectively. The ground-truth variables will be indicated with a star on top of their notations \mathcal{G}^* . We assume throughout that all distributions possess densities $p(\mathbf{x}_t)$ w.r.t. the Lebesgue measure. We use the same notation as in [12], where $\text{Pa}_{\mathcal{G}}^i(< t)$ refers to the parents of node i in \mathcal{G} at previous time $t - \tau$ with $\tau \leq L$ (lagged parents) and $\text{Pa}_{\mathcal{G}}^i(t)$ to the parents at the current time t (instantaneous parents $\tau = 0$).

Consider the MTS $(\mathbf{x}_t)_{t \in \mathcal{T}} = (x_t^i)_{i \in \mathbf{V}, t \in \mathcal{T}}$ where $|\mathbf{V}| = d$ number of components of MTS $(\mathbf{x}_t)_{t \in \mathcal{T}}$ and \mathcal{T} is time index set. The MTS $(\mathbf{x}_t)_{t \in \mathcal{T}}$ is aligned with a temporal causal graph \mathcal{G} elucidating its generative process. Each component of the MTS at time t is represented by a singular node within the graph \mathcal{G} which is defined as follows:

Definition 2.1. (Temporal Causal Graph) The temporal causal graph, associated with the MTS $(\mathbf{x}_t)_{t \in \mathcal{T}}$, is defined by a DAG $\mathcal{G} = (\mathbf{V}, E)$ and a fixed maximum lag L . Its vertices \mathbf{V} consists of the set of components x^1, \dots, x^d at each time $t - L, \dots, t$. The edges E of the graph are defined as follows: $\forall \tau \in [1 : L]$ variables $x_{t-\tau}^i$ and x_t^j are connected by a lag-specific directed link $x_{t-\tau}^i \rightarrow x_t^j$ in \mathcal{G} pointing forward in time if and only if x^i at time $t - \tau$ causes x^j at time t . Then the coefficient $[\mathcal{G}_\tau]_{ij}$ associated with the adjacency matrix $\mathcal{G}_\tau \in \mathcal{M}_d(\mathbb{R})$ will be non-null and $x^i \in \text{Pa}_{\mathcal{G}}^j(< t)$ if $\tau \neq 0$. For instantaneous links ($\tau = 0$), we can not have self loops i.e. $i \neq j$. If $\tau = 0$, we have an edge $x_t^i \rightarrow x_t^j$ and $x^i \in \text{Pa}_{\mathcal{G}}^j(t)$ if and only if x^i at time t causes x^j at time t .

MTS composed of multiple regimes. A MTS can exhibit a single regime (as assumed in prior works like Rhino [12] and DYNOTEARS [27]) or K different regimes, as in our approach. Each regime can be seen as a MTS temporal block with a minimum duration, denoted as ζ . Regimes occur sequentially, with the condition that a second regime can only commence after a duration of at least ζ from the initiation of the preceding regime, each regime will have its own temporal causal graph.

Definition 2.2. (MTS with multiple regimes) We say that MTS $(\mathbf{x}_t)_{t \in \mathcal{T}} = (x_t^i)_{i \in \mathbf{V}, t \in \mathcal{T}}$ is composed of K disjoint regimes if it exists a unique time partition $\mathcal{E} = (\mathcal{E}_u)_{u \in \{1, \dots, K\}}$, such that: $\cap_{u=1}^K \mathcal{E}_u = \emptyset$, $\mathcal{T} = \cup_{u=1}^K \mathcal{E}_u$ and $\forall u \in \{1, \dots, K\}$, the MTS $(\mathbf{x}_t)_{t \in \mathcal{E}_u}$ is stationary and associated with a unique temporal causal graph \mathcal{G}^u .

Notably, the regime v (where $v = u + 1$) begins at least ζ samples after the start of regime u and also persists for a minimum of ζ samples. Additionally, if regime u reoccurs, its duration in the second appearance is also no less than ζ samples (Minimum regime duration). All the indices corresponding to the first and second appearances of this regime u are stored in \mathcal{E}_u .

It is crucial to note that \mathcal{G}^u are regime-dependent, meaning that graphs vary across different regimes i.e., $\mathcal{G}^u \neq \mathcal{G}^v$. In the rest of our paper, we note $\mathcal{G} = (\mathcal{G}^u)_{u \in \{1, \dots, K\}}$ the set of temporal causal graph associated with a MTS $(\mathbf{x}_t)_{t \in \mathcal{T}}$ composed of K regimes. Each regime u , is associated with a temporal causal graph \mathcal{G}^u defined above in definition 2.1.

Structural Equation Model (SEM) for MTS composed of multiple regimes. We now propose a novel functional form for SEM that incorporates linear or non-linear relations, instantaneous links and multiple regimes. Specifically, we have $\forall u \in \{1, \dots, K\}, \forall t \in \mathcal{E}_u$:

$$x_t^i = g_i^u(\mathbf{Pa}_{\mathcal{G}^u}^i(< t), \mathbf{Pa}_{\mathcal{G}^u}^i(t)) + \epsilon_t^i, \quad (1)$$

where g_i^u is a general differentiable linear or non-linear function and where $\epsilon_t^i \sim \mathcal{N}(0, 1)$, follows to a normal distribution. By assuming causal Markov property, we can define the associated Causal graphical model (CGM), with $\mathbf{x}_{<t}$ symbolises $\{\mathbf{x}_{t-L}, \dots, \mathbf{x}_{t-1}\}$, $\forall u \in \{1, \dots, K\}, \forall t \in \mathcal{E}_u$:

$$p(\mathbf{x}_t | \mathbf{x}_{<t}, \mathcal{G}^u) = \prod_{i=1}^d p(x_t^i | \mathbf{Pa}_{\mathcal{G}^u}^i(< t), \mathbf{Pa}_{\mathcal{G}^u}^i(t)). \quad (2)$$

When the MTS consist of K unknown regimes, it cannot be represented by a single DAG. A new formulation of the distribution p describing the CGM in such scenarios is as follows:

$$p(\mathbf{x}_t | \mathbf{x}_{<t}) = \sum_{u=1}^K p(z_{t,u}) \cdot p(\mathbf{x}_t | \mathbf{x}_{<t}, \mathcal{G}^u), \quad (3)$$

where $p(\mathbf{x}_t | \mathbf{x}_{<t}, \mathcal{G}^u)$ is specified in Equation (2), while $p(z_{t,u})$ models the probability of \mathbf{x}_t belonging to regime u (the variable z_t introduced in Figure 3). As we explained in the definition 2.2, the regimes are non-overlapping hence the $p(z_{t,u}) = \mathbb{1}_{\mathcal{E}_u}(t)$ is an indicator function, defined as $\mathbb{1}_{\mathcal{E}_u}(t) = 1$ if $t \in \mathcal{E}_u$ and 0 otherwise. Previous works assume prior knowledge of time partition \mathcal{E} or report a summary causal graph [16], falling short of elucidating the full temporal causal graph. In the next section we will present CASTOR, an optimization based method for temporal causal structure learning tailored for MTS with multiple regimes, as introduced above.

3 CASTOR: Causal temporal regime structure learning

In this section, we present a novel approach designed to learn the set of DAGs $\mathcal{G} = (\mathcal{G}^u)_{u \in \{1, \dots, K\}}$, the total number of regimes K , and the associated regime indices $\mathcal{E} = (\mathcal{E}_u)_{u \in \{1, \dots, K\}}$ from a MTS $(\mathbf{x}_t)_{t \in \mathcal{T}}$ composed of multiple unknown regimes. Sections 3.1 and 3.2 delineate the regime learning procedure and the graph learning procedure.

Our objective is now to learn simultaneously K , $\mathcal{E} = (\mathcal{E}_u)_{u \in \{1, \dots, K\}}$ and their DAGs $\mathcal{G} = (\mathcal{G}^u)_{u \in \{1, \dots, K\}}$ that maximise the $\log p(\mathbf{x}_{0:|\mathcal{T}|})$ defined as follows:

$$\log p(\mathbf{x}_{0:|\mathcal{T}|}) = \sum_{t=0}^{|\mathcal{T}|} \log \sum_{u=1}^K \mathbb{1}_{\mathcal{E}_u}(t) \cdot p(\mathbf{x}_t | \mathbf{x}_{<t}, \mathcal{G}^u). \quad (4)$$

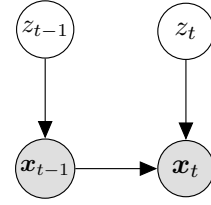


Figure 2: The graphical model assumed by CASTOR for lag $L = 1$, the observed variables are depicted in grey, while the latent variable $z_t \in \mathbf{R}^{N_w}$ remains uncolored. \mathbf{x}_t being associated with regime u if $z_{t,u} = 1$.

Learning the DAGs $\mathcal{G} = (\mathcal{G}^u)_{u \in \{1, \dots, K\}}$, concurrently entails the estimation of the regime distribution $p(\mathbf{x}_t \mid \mathbf{x}_{<t}, \mathcal{G}^u)$. We model CASTOR’s estimation of the joint density of the u^{th} regime by:

$$f^u(\mathbf{x}_t) := \prod_{i=1}^d f_i^u(\mathbf{Pa}_{\mathcal{G}^u}^i(<t), \mathbf{Pa}_{\mathcal{G}^u}^i(t)), \quad (5)$$

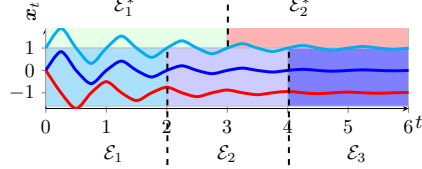
where f^u is a distribution family. It is important to highlight that while f^u can in theory be any distribution, in this particular study, we assume normal noise, used by many works ([16, 27]) and for which they showed the identifiability of causal graphs for one regime [16, 28]. As a result from SEM Eq (1), our distribution f^u will be a Gaussian distribution.

The learning problem is challenging as the regime indices remain unknown. The presence of the sum within the log terms in Eq (4) renders the log likelihood intractable. The EM algorithm [9] is well-suited for tackling this specific problem, it introduces new variables $\gamma_{t,u}$ to model regime participation and alternates between regime learning (E-step) and graph learning (M-step), thereby transforming the log likelihood to the following form:

$$\log p(\mathbf{x}_{0:|\mathcal{T}|}) = \sum_{t=0}^{|\mathcal{T}|} \sum_{u=1}^K \gamma_{t,u} \log \left(\mathbb{1}_{\mathcal{E}_u}(t) \cdot f^u(\mathbf{x}_t) \right).$$

However, the term within the logarithm may be zero, leading to divergence in our log-likelihood, also applying EM necessitates prior knowledge of the number of regimes. In our scenario, we operate under the assumption that this information is not available.

To address the divergence problem of our log-likelihood, we aim to learn functions that solve the divergence problem, but also robust against random regime switching for a given sample \mathbf{x}_t . We want a sample \mathbf{x}_t , if belonging to regime u in the current iteration, to be assigned to the neighboring regimes $(u-1, u+1)$ or the same regime u in the next iteration. We employ the soft-max function $\pi_t(\alpha_u) = \frac{\exp(\alpha_{u,1}t + \alpha_{u,0})}{\sum_{j=1}^{N_w} \exp(\alpha_{j,1}t + \alpha_{j,0})}$ (which is a function of a learnable parameter α_u and time index t).



For the second challenge; the unavailability of the number of regimes, K , CASTOR initially divides the MTS into $N_w > K$ equal time windows in the initialisation step (the length of the initialized windows is greater than ζ minimum regime duration), where each window represents one initial regime estimate. Our initialization scheme builds some initial **pure** regimes (regimes composed of samples from the same ground truth regime) and other **impure** ones (regimes composed of samples from two neighboring ground truth regimes).

Figure 3: Example of initialization with $N_w = 3$ windows, \mathcal{E}_1 and \mathcal{E}_3 are pure regimes while \mathcal{E}_2 is impure (composed of samples from two ground-truth regimes \mathcal{E}_1^* and \mathcal{E}_2^* , $K = 2$).

The log-likelihood of Eq (4) becomes:

$$\log p(\mathbf{x}_{0:|\mathcal{T}|}) = \sum_{t=0}^{|\mathcal{T}|} \sum_{u=1}^{N_w} \gamma_{t,u} \log \left(\pi_t(\alpha_u) \cdot f^u(\mathbf{x}_t) \right).$$

After our initialization scheme, we start with some **pure** regimes and **impure** regimes due to the fact that our initial windows are sufficiently small. CASTOR estimates the graphs (by learning $f^u(\mathbf{x}_t)$) for the different initial regimes and also learns the parameters α_u that maximizes the alignment between $\gamma_{t,u}$ (rectangular function) and $\pi_t(\alpha_u)$ (example on Figure 4) using the M-step (subsection 3.2). This alignment is desirable to ensure stability in the assignment of the samples.

3.1 Expectation step: Regime learning

During the E-step, CASTOR updates $\gamma_{t,u}$ (as shown in Eq (6), derivation details in Appendix D), the probability of \mathbf{x}_t belonging to regime u depends on two factors, the position of \mathbf{x}_t within the current regime and whether the current regime is **pure or impure**.

$$\gamma_{t,u} = \frac{p(z_{t,u} = 1) p(\mathbf{x}_t \mid \mathbf{x}_{<t}, z_{t,u} = 1, \mathbf{G}_{\{0:L\}}^u)}{\sum_{j=1}^{N_w} p(z_{t,j} = 1) p(\mathbf{x}_t \mid \mathbf{x}_{<t}, z_{t,j} = 1, \mathbf{G}_{\{0:L\}}^j)} = \frac{\pi_t(\alpha_u) f^u(\mathbf{x}_t)}{\sum_{j=1}^{N_w} \pi_t(\alpha_j) f^j(\mathbf{x}_t)} \propto \pi_t(\alpha_u) f^u(\mathbf{x}_t) \quad (6)$$

Case 1: \mathbf{x}_t belongs to regime u in the current iteration, \mathbf{x}_t is far from the border and regime u is pure. In this case, $\pi_t(\alpha_u)$ is high (case of $\pi_{t \in \llbracket 0, 300 \rrbracket}(\alpha_0)$ in the example of Figure 4) and the

graph in u is meaningful because it was learned on a pure regime, so $f^u(\mathbf{x}_t)$ is also high, thus $\gamma_{t,u} \propto \pi_t(\alpha_u) f^u(\mathbf{x}_t)$ Eq (6) stays maximal for \mathbf{x}_t to remain in regime u in the next iteration.

Case 2: \mathbf{x}_t belongs to regime u in the current iteration, \mathbf{x}_t is near the border and regime u is pure. In this case, $\pi_t(\alpha_u)$ and $\pi_{t,u+1}(\alpha_{u+1})$ are roughly close ($\pi_{t \in [350, 500]}(\alpha_0)$ and $\pi_{t \in [350, 500]}(\alpha_1)$ in Figure 4), $f^u(\mathbf{x}_t)$ is still high, because the graph was learned on a pure regime, thus $\gamma_{t,u}$ stays maximal for \mathbf{x}_t to remain in regime u in the next iteration.

Case 3: \mathbf{x}_t belongs to regime $u+1$ in the current iteration, \mathbf{x}_t is near the border and regime $u+1$ is impure. In this case, $\pi_{t,u}(\alpha)$ and $\pi_{t,u+1}(\alpha)$ are roughly close ($\pi_{t \in [501, 650]}(\alpha_0)$ and $\pi_{t \in [501, 650]}(\alpha_1)$ in Figure 4), however $f^u(\mathbf{x}_t) > f^{u+1}(\mathbf{x}_t)$, because the graph of regime u is more meaningful than the graph of regime $u+1$, thus $\gamma_{t,u} > \gamma_{t,u+1}$ which makes the sample \mathbf{x}_t switch regimes from $u+1$ to u in the next iteration.

Case 4: \mathbf{x}_t belongs to regime $u+1$ in the current iteration, \mathbf{x}_t is far from the border and regime $u+1$ is impure. In this case ($t \in [650, 850]$ in the example of Figure 4), we cannot say with certainty whether \mathbf{x}_t switches regime or not in the next iteration, but because the pure regime u grows after each iteration, \mathbf{x}_t will soon enough be in the border of regime $u+1$ which takes us back to 3.

For simplicity reasons, we explicit these cases from one border but the same thing happens in the other border which accelerates convergence. If a sample \mathbf{x}_t belongs to regime u , it will never be allocated to a non neighboring regime v due to the fact that $\pi_t(\alpha_u) \gg \pi_t(\alpha_v)$ and $f^u(\mathbf{x}_t) \gg f^v(\mathbf{x}_t)$.

Example. In the example depicted in Figure 4, after learning the graphs and parameters α_u for the first iteration where the regimes are equal windows of 500 data points. The samples \mathbf{x}_t , where $t \in [350, 500]$ belonging to regime 0 in the previous iteration, are more likely to stay in regime 0 or transition to the neighboring regime 1 ($\pi_{t \in [350, 500]}(\alpha_1)$ same range as $\pi_{t \in [350, 500]}(\alpha_0)$) than the non neighboring regime 2 ($\pi_{t \in [350, 500]}(\alpha_2)$ almost 0).

After updating $\gamma_{t,u}$, for each sample \mathbf{x}_t , CASTOR assigns a value of 1 to the most probable regime u (with the highest $\gamma_{t,u}$), and 0 to others. Additionally, CASTOR filters out regimes with insufficient samples (fewer than ζ , the minimum regime duration, defined as a hyper-parameter). Discarded regime samples are then reassigned to the nearest regime in terms of probability $\gamma_{t,u}$ in the subsequent iteration which is in general a neighboring regime ensured by the way we set up the probability $\gamma_{t,u} \propto \pi_{t,u}(\alpha) f^u(\mathbf{x}_t)$.

3.2 Maximization step: Graph learning

CASTOR utilizes the regime indices $\gamma_{t,u}$ learned in the E-step to estimate the DAGs for each regime and learn the parameters α that align $\pi_t(\alpha_u)$ with $\gamma_{t,u}$ by maximizing the following equation:

$$\sup_{\theta, \alpha} \frac{1}{|\mathcal{T}|} \sum_{u=1}^{N_w} \sum_{t=0}^{|\mathcal{T}|} \gamma_{t,u} \log \pi_t(\alpha_u) f^u(\mathbf{x}_t) - \lambda |\mathcal{G}^u|, \text{ s.t., } \mathbf{G}_0^u \text{ is a DAG.}$$

The maximization of the aforementioned equation can be decomposed into two distinct maximization problems. The first problem focuses on aligning $\pi_t(\alpha_u)$ with $\gamma_{t,u}$, while the second one involves estimating DAGs for every regime:

$$\underbrace{\sup_{\alpha} \frac{1}{|\mathcal{T}|} \sum_{u=1}^{N_w} \sum_{t=1}^{|\mathcal{T}|} \gamma_{t,u} \log(\pi_t(\alpha_u))}_{\text{Regime indices alignment}} \quad \underbrace{\mathcal{S}(\mathcal{G}, \mathcal{E}) := \sup_{\theta} \frac{1}{|\mathcal{T}|} \sum_{u=1}^{N_w} \sum_{t \in \mathcal{E}_u} \log f^u(\mathbf{x}_t) - \lambda |\mathcal{G}^u|}_{\text{Graph learning}}, \text{ s.t., } \mathbf{G}_0^u \text{ is a DAG,} \quad (7)$$

where θ stands for the parameters of CASTOR, $\alpha = \{\alpha_u, \forall u \in [1, N_w]\}$, $|\mathcal{G}^u|$ is the number of edges in the temporal causal graph of regime u and we note $\mathcal{S}(\mathcal{G}, \mathcal{E})$ the score function of CASTOR. The first term in CASTOR's score function is the averaged log-likelihood over data while the second

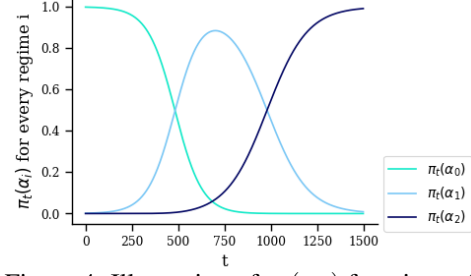


Figure 4: Illustration of $\pi_t(\alpha_u)$ functions after the first iteration of CASTOR. We are in the setting of MTS comprising 1500 samples with two unknown ground-truth regimes. The ground-truth partition of the first regime $\mathcal{E}_1 = \{0, \dots, 799\}$, while the second ground-truth partition is $\mathcal{E}_2 = \{800, \dots, 1500\}$. $\gamma_{t,u}$ are initialized as equal windows of length 500, the first and last windows are **pure**, but the middle one is **impure**.

term is a penalty term with positive small coefficient λ that controls the sparsity constraint. We further impose an acyclicity constraint on the adjacency matrix \mathbf{G}_0^u of instantaneous links. The other adjacency matrices $\mathbf{G}_\tau^u \in \{[1:L]\}$ are inherently acyclic by definition, because these matrices establish links between variables at time t and their time-lagged parents at time $t - \tau$. It is worth noting that the optimization for [regime alignment](#) remains the same for both linear and nonlinear causal relationships. However, the [graph learning](#) problem differs between these two settings.

3.3 Linear case

In the case of linear causal relationships, the SEM (Eq (1)) can then be articulated as follows: $\forall u \in \{1, \dots, K\}, \forall t \in \mathcal{E}_u : \mathbf{x}_t = \mathbf{x}_t \mathbf{G}_0^u + \sum_{\tau=1}^L \mathbf{x}_{t-\tau} \mathbf{G}_\tau^u + \epsilon_t$, where $\epsilon_t \sim \mathcal{N}(0, I)$. We thus have $\forall u \in \{1, \dots, K\}, \forall t \in \mathcal{E}_u : \mathbf{x}_t | \mathbf{x}_{<t} \sim \mathcal{N}(\mathbf{x}_t \mathbf{G}_0^u + \sum_{\tau=1}^L \mathbf{x}_{t-\tau} \mathbf{G}_\tau^u, I)$. Employing CASTOR's score function gives rise to the following minimization problem (Details of the computation can be found in the Appendix D).

$$\min_{\mathcal{G}} \frac{1}{|\mathcal{T}|} \sum_{u=1}^{N_w} \sum_{t=1}^{|\mathcal{T}|} \gamma_{t,u} \left\| \mathbf{x}_t - \left(\mathbf{x}_t \mathbf{G}_0^u + \sum_{\tau=1}^L \mathbf{x}_{t-\tau} \mathbf{G}_\tau^u \right) \right\|_F^2 + \lambda |\mathcal{G}^u| + \frac{\rho}{2} h(\mathbf{G}_0^u)^2 + \alpha h(\mathbf{G}_0^u), \quad (8)$$

where \mathcal{G} stands for $\mathcal{G} = (\mathcal{G}^u)_{u \in \{1, \dots, K\}}$ and α, ρ characterize the strength of the DAG penalty. The function $h(\mathbf{G}) = \text{tr}(e^{\mathbf{G} \odot \mathbf{G}}) - d$ corresponds to the acyclicity constraints proposed in [45] (\odot is the Hadamard product). For example, let \mathbf{G}_0 be the adjacency graph for instantaneous relation. The constrain condition requires $h(\mathbf{G}_0) = 0$. We employ an augmented Lagrangian method [6, 22, 27, 45] to address the optimization challenge that incorporates the acyclicity constraints.

3.4 Non-linear case

In case of non-linear causal relationships between the component of the MTS $(\mathbf{x}_t)_{t \in \mathcal{T}}$. We have to estimate the parameters of the distribution f^u (Eq (7)), recognizing that the generative process follows a non-linear pattern, as described in the SEM (Eq (1)).

Based on the Eq (1), we have $\forall u \in \{1, \dots, K\}, \forall t \in \mathcal{E}_u : \mathbf{x}_t | \mathbf{x}_{<t} \sim \mathcal{N}(g_t^u(\mathbf{Pa}_{\mathcal{G}^u}^i(<t), \mathbf{Pa}_{\mathcal{G}^u}^i(t)), 1)$, implies that the distribution we aim to estimate is a Gaussian distribution. We employ Neural Networks (NN) to accommodate the non-linearity introduced in our problem formulation, similarly to what is done in [6, 22, 46]. For every regime u , a NN_i^u is used to model the parameters of the distribution f_i^u . For each time step t , we aggregate all time-lagged variables to form a single time lag vector, denoted as $\mathbf{x}_t^{\text{lag}} = [\mathbf{x}_{t-1} | \dots | \mathbf{x}_{t-L}]$, which encompasses the lagged data. We employ \mathbf{x}_t and $\mathbf{x}_t^{\text{lag}}$ as inputs for different neural networks $\text{NN}_i^u, \forall (i, u) \in \{1, \dots, d\} \times \{1, \dots, N_w\}$ and gets \hat{x}_t^i as output (an estimation of x_t^i), with the objective of estimating the parameters of the distributions f_i^u .

Mathematically, our NNs are formulated as follows: $\forall i \in \{1, \dots, d\} : \text{NN}_i^u(\mathbf{x}_t, \mathbf{x}_t^{\text{lag}}) = \psi_i^u(\phi_i^u(\mathbf{x}_t), \phi_i^{u, \text{lag}}(\mathbf{x}_t^{\text{lag}}))$, where ψ_i^u are neural networks composed of locally connected layers introduced in [46] and activation functions, $\phi_i^u, \phi_i^{u, \text{lag}}$ composed of linear layers and sigmoid functions. The locally connected layers help to encode the variable dependencies in the first layer.

For a given node i , the instantaneous and time-lagged interactions with another node j can be succinctly captured by examining the norms of the corresponding columns j in the weight matrices of the initial layers such that: $[\mathbf{G}_0^u]_{ij} = \|\Theta_i^u(\text{column } j)\|_2, [\mathbf{G}_\tau^u]_{ij} = \|\Theta_i^{u, \text{lag}}(\text{column}((\tau - 1) \cdot d + j))\|_2$.

Θ_i^u and $\Theta_i^{u, \text{lag}}$ represent the parameters of the first layer of the NNs $\phi_i^u, \phi_i^{u, \text{lag}}$ respectively. As we know the matrix $\Theta_i^{\text{lag}} \in \mathcal{M}_{d, d \cdot L}(\mathbb{R})$, it has $d \cdot L$ columns (where L is the maximum number of lag as defined above). Finally, introducing NNs and elaborating on the mathematical expressions for the maximization step in Eq (7) leads to the following equivalent minimization problem (derivation details in Appendix D):

$$\min_{\theta, \mathcal{G}} \frac{1}{|\mathcal{T}|} \sum_{u=1}^{N_w} \sum_{t=1}^{|\mathcal{T}|} \sum_{i=1}^d \gamma_{t,u} \mathcal{L}(x_t^i, \psi_i^u(\phi_i^u(\mathbf{x}_t), \phi_i^{u, \text{lag}}(\mathbf{x}_t^{\text{lag}}))) + \lambda |\mathcal{G}^u| + \frac{\rho}{2} h(\mathbf{G}_0^u)^2 + \alpha h(\mathbf{G}_0^u),$$

where \mathcal{L} is a least squares loss, θ summarises all the network parameters and $\mathcal{G} = (\mathcal{G}^u)_{u \in \{0, \dots, K\}}$. We use the same technique as described above for the linear case for the acyclicity constraint, we add

the augmented Lagrangian term $\frac{\rho}{2}h(\mathbf{G}_0^u)^2 + \alpha h(\mathbf{G}_0^u)$ to our optimization problem. Algorithm 1 overviews our CASTOR model for both linear and nonlinear causal relationships.

4 Theoretical guarantees

In this section, we present the theoretical guarantees on the identifiability of DAGs and regime indices within the CASTOR framework. The theorem 4.1 (proof in the Appendix F) states that reaching the optimal solution of Eq (4) establish the identifiability of the regimes and the DAGs. The table 8 in Appendix F demonstrates that our assumptions are commonly shared among various state-of-the-art models in causal discovery. Additionally, it highlights that CASTOR relaxes certain assumptions of existing methods, such as stationarity.

Theorem 4.1. *We assume that each regime has enough data, the penalty coefficients in Eq (8-3.4) are sufficiently small, CASTOR SEMs satisfy the causal Markov property, minimality and sufficiency (Appendix F for more details). If CASTOR learns K , $\mathcal{E} = (\mathcal{E}_u)_{u \in \{1, \dots, K\}}$ and their DAGs $\mathcal{G} = (\mathcal{G}^u)_{u \in \{1, \dots, K\}}$ that maximize the log-likelihood of Eq (4):*

$$\log p(\mathbf{x}_{0:|\mathcal{T}|}) = \sum_{t=0}^{|\mathcal{T}|-1} \log \sum_{u=1}^K \mathbb{1}_{\mathcal{E}_u}(t) \cdot p(\mathbf{x}_t | \mathbf{x}_{<t}, \mathcal{G}^u).$$

Then all the regimes are pure and identifiable and for every pure regime the DAGs are also identifiable in the linear and non-linear case.

Proof Sketch (Full proof in the Appendix F.1). First we show by contradiction that for any estimation $(\hat{\mathcal{G}}, \hat{\mathcal{E}})$ of set of regime partitions and DAGs, if the score defined by CASTOR (graph learning problem of Eq (7)) for that estimation $\mathcal{S}(\hat{\mathcal{G}}, \hat{\mathcal{E}})$ is optimized the regime will all be pure and identified. Then we show that for all the identified regimes the DAGs are identified in the linear case using the same arguments as [28] and in the non linear case using the Theorem 2 of [29]. Furthermore, we demonstrate that for any sub-optimal $(\hat{\mathcal{G}}, \hat{\mathcal{E}}) : \mathcal{S}(\mathcal{G}^*, \mathcal{E}^*) > \mathcal{S}(\hat{\mathcal{G}}, \hat{\mathcal{E}})$,

The theorem highlights that inaccuracies in identifying causal structures or real regimes lead to a sub-optimal estimation score. When the log-likelihood is optimized, CASTOR successfully identifies the actual regimes and recovers true causal graphs. Nevertheless, convergence to sub-optimal outcomes may occur. However, the theorem does not provide information about the relationship between two sub-optimal solutions. Specifically, if our defined score function has an ordering property, meaning that the scores of two estimations can be ranked, can we assert that the closest estimation to the optimal solution in terms of Kullback–Leibler divergence has the higher score? We demonstrate that this statement is true and present the following theorem, *proved in the Appendix F.1*:

Theorem 4.2. *Assuming the same conditions as in Theorem 4.1, we have for any estimation (Appendix F for more details). We have for any estimations $(\mathcal{G}, \mathcal{E})$ and $(\mathcal{G}', \mathcal{E}')$ such that $(\mathcal{G}, \mathcal{E})$ is closer to the optimal solution $(\mathcal{G}^*, \mathcal{E}^*)$ than $(\mathcal{G}', \mathcal{E}')$ in terms of Kullback–Leibler, we have: $\mathcal{S}(\mathcal{G}, \mathcal{E}) > \mathcal{S}(\mathcal{G}', \mathcal{E}')$.*

5 Experiments

5.1 Synthetic data

Data generation. We perform extensive experiments to evaluate the performance of CASTOR in controlled settings with synthetic datasets (Details of the data generation can be found in Appendix E.1). For groundtruth graph generation, we employ the Barabási-Albert [5] model with a degree of 4 to establish instantaneous links, while we utilize the Erdős–Rényi [26] random graph model with degrees ranging from 1 to 2 for time-lagged relationships. In the case of non-linear relationships, the functions g_i^u defined in Eq (1) include random weights generated from a uniform distribution over the interval]0,2], coupled with activation functions selected randomly from the set {Tanh, LeakyReLU, ReLU}. We focus here on scenarios with a single time lag $L = 1$, although additional experiments involving multiple lags are detailed in Appendix. The duration of each regime is chosen randomly from the set {300, 400, 500, 600}. We examine varying numbers of nodes, specifically {5, 10, 20, 40} for linear cases, {10, 20} for non-linear cases, and generated time series with different regime counts $K \in \{2, 3, 4, 5\}$. Each experiment (corresponding to one combination of K regimes and d nodes) was repeated three times to compute the standard deviation, all combinations yield to more than 60 different datasets.

Benchmarks. Our model’s performance is benchmarked against multiple baselines, including causal discovery methods specifically tailored for the setting of MTS composed of multiple regimes, such as CD-NOD [16] and RPCMCI [37]. It is worth noting that CD-NOD returns a summary graph (as

Table 1: Average F1 Scores on regimes for different models and settings for linear causal relationships. Here, d denotes the number of nodes, K the number of regimes, ‘‘Split’’ specifies whether the regime split is automatic (A) or manual (M), and ‘‘Type’’ categorizes the graph as either a window (W) or summary (S). ‘‘Inst.’’ refers to instantaneous links and ‘‘Lag’’ to time-lagged edges.

Model	Split	Type	$d = 10$						$d = 40$					
			$K = 2$		$K = 3$		$K = 4$		$K = 2$		$K = 3$		$K = 4$	
			Inst.	Lag	Inst.	Lag	Inst.	Lag	Inst.	Lag	Inst.	Lag	Inst.	Lag
VARLINGAM	M	W	18.2 \pm 3.8	10.4 \pm 7.8	11.0 \pm 6.4	5.01 \pm 1.4	9.70 \pm 1.8	5.10 \pm 3.1	8.40 \pm 1.2	1.2 \pm 0.1	9.83 \pm 0.9	1.13 \pm 0.8	10.9 \pm 3.1	1.43 \pm 0.6
Rhino	M	W	62.4 \pm 10.	40.7 \pm 4.4	54.8 \pm 3.9	44.4 \pm 5.0	50.7 \pm 2.5	43.0 \pm 6.6	0.00 \pm 0.0	21.1 \pm 2.1	0.00 \pm 0.0	20.8 \pm 1.3	0.00 \pm 0.0	22.8 \pm 0.9
Rhino w/o hist	M	W	90.2 \pm 3.4	58.5 \pm 2.3	87.5 \pm 3.6	53.5 \pm 2.2	88.2 \pm 1.7	61.8 \pm 2.9	0.00 \pm 0.0	44.1 \pm 1.2	0.00 \pm 0.0	38.4 \pm 3.6	0.00 \pm 0.0	39.1 \pm 1.3
PCMCi+	M	W	81.1 \pm 7.4	89.5 \pm 3.8	80.4 \pm 4.5	83.6 \pm 3.5	77.7 \pm 1.8	77.6 \pm 3.2	55.2 \pm 3.6	85.4 \pm 4.1	54.1 \pm 5.4	84.6 \pm 2.6	53.7 \pm 3.2	86.1 \pm 1.8
DYNOTEARS	M	W	100.0 \pm 0.0	100.0 \pm 0.0	96.9 \pm 2.5	100.0 \pm 0.0	99.6 \pm 0.9	99.8 \pm 1.4	100.0 \pm 0.0	100.0 \pm 0.0	97.4 \pm 1.7	98.8 \pm 0.2	97.3 \pm 0.8	97.9 \pm 0.6
RPCMCI	A	W	-	42.3 \pm 11.	-	18.8 \pm 2.5	-	-	-	42.1 \pm 3.5	-	18.4 \pm 14.	-	
CASTOR	A	S	100.0 \pm 0.0	100.0 \pm 0.0	97.3 \pm 2.5	100.0 \pm 0.0	99.3 \pm 0.9	98.0 \pm 1.4	98.3 \pm 1.7	100.0 \pm 0.0	98.2 \pm 1.2	99.8 \pm 0.2	98.3 \pm 0.4	98.9 \pm 0.9
CD-NOD	A	S		20.2		11.4		38.8		0		11.3		5.57
CASTOR	A	S		100		100		97.9		100		99.8		99.2

defined in Appendix E.7). Therefore, we generated a summary causal graph from CASTOR’s output to compare the two models in the context of summary graph settings. CASTOR is also compared with models designed for MTS with a single regime, namely Rhino [12] (with and without historically dependent noise, referred to as ‘‘Rhino’’ and ‘‘Rhino w/o’’ in the table 1), PCMCi+ (with Partial correlation test for linear relationships and with GPDC non linear conditional independence test for non linear relationships) [34], DYNOTEARS [27], VARLINGAM [18]. Given that these models cannot deal with multiple regimes, to make the evaluation fair, we put them in a more favorable position and provide these models with the true regime partition information. This is done by training the aforementioned models on each pure regime separately (regime governed by the same graph).

Results. Table 1 presents the results for linear case, while Figure 5 summarizes the results for the non-linear setting. CASTOR outperforms all the baselines, including those designed for MTS with multiple regimes, such as RPCMCI and CD-NOD (Table 1). Additionally, CASTOR exceeds the performance of other methods that assume stationarity (Table 1 and Figure 5) and even if they are given the advantage of accessing regime ground truth partitions beforehand (by training the models on each pure regime separately).

Discussion. RPCMCI necessitates prior knowledge of the number of regimes and the maximum number of transitions, and with this input, it only infers time-lagged relations. Even with this detailed information, RPCMCI struggles to achieve convergence, particularly in settings with more than 3 different regimes due to its assumption of only inferring time-lagged relations. This assumption makes our scenario more complex for this algorithm, impacting both regime learning and graph inference tasks. The comparison with CD-NOD on graph learning and also regime detection was provided in our first submission in the Appendix E.6, E.7. The results show that CASTOR outperforms CD-NOD, which is understandable because, CD-NOD learns one summary graph for the whole MTS and also expects only a few variables of the graph to be affected by the regime change (This assumption may not hold true in real scenarios such as epileptic seizures or climate science). However, CASTOR does not have this assumption (few variables are affected by the regime change) and also learns one graph per regime. Although our settings are identifiable, PCMCi+ infers a Markov equivalent class for the instantaneous links, which explains its performance deterioration, particularly in instantaneous relations and with a higher number of nodes. Rhino, which is a state-of-the-art causal discovery method for nonlinear relationships, faces challenges in the absence of historical dependent noises (as confirmed by Figure 4 on page 24 of the Rhino paper). Moreover, Rhino utilizes ConvertibleGNN with Normalizing flows to learn the causal graphs. To train this model, a minimum of 50 time series of length 200 (10000 samples), all sharing the same causal graph. In contrast, our dataset consists of regimes that do not exceed 600 samples. This difference in dataset characteristics poses challenges for Rhino’s performance in our scenario. Finally, DYNOTEARS faces challenges in non-linear causal

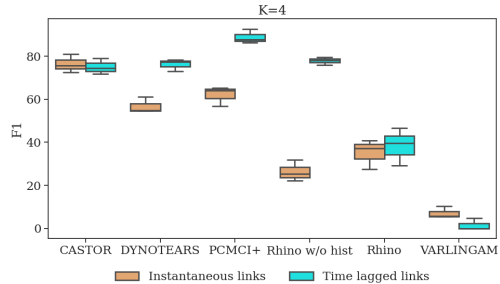


Figure 5: F1 scores by Models for 20 nodes and 4 regimes. Orange indicates performance on instantaneous links, and sky-blue signifies performance on time-lagged relationships.

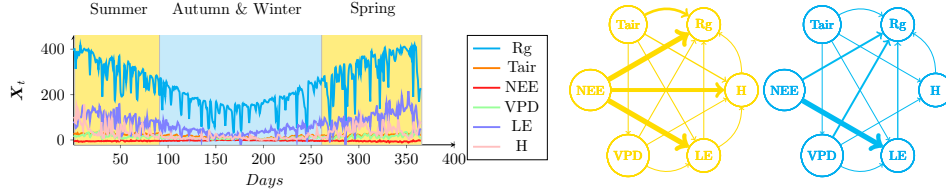


Figure 6: Applying CASTOR to Biosphere atmosphere data. CASTOR identifies two regimes with distinct graphs. Here, only instantaneous links are shown, with the blue graph corresponding to the blue regime and the yellow one to the yellow regime.

relationships (specially instantaneous links) as expected due to its assumption of considering only linear causal relation. [Additional results and evaluations using other metrics, such as SHD, that confirm the above findings are available in Appendix E.4 and E.5.](#) The comparison with CD-NOD [16] and KCP [2] on the regime detection task is presented in Appendix E.7.

5.2 Web activity dataset

We now evaluate CASTOR on two stacked IT monitoring time series datasets (firstly introduced by [8], details and analysis of the challenges of these datasets are in Appendix E.2), each comprising 1106 timestamps and 7 nodes, sourced from EasyVista. The web activity data is challenging, because it could present missing values, misaligned time series and partially sleeping time series due to inactivity of certain servers. IT experts are not sure that this data satisfies causal sufficiency assumption. Ait-Bachir, Ali, et al. [1] present a study on the performance of causal discovery method on this data and shows the same range of performance. We compared our method to a subset of the best models mentioned in the benchmark subsection. As it is evident from Table 2, CASTOR proficiently identifies the exact number of regimes and their indices. On regime 2, CASTOR (with linear relationships), PCMCi+ and DYNOTEARS outperform Rhino and CASTOR non-lin (uses NN for non linear relationships). However, in regime 1, CASTOR non-linear and Rhino outperform all other models. This superiority can be attributed to the fact that CASTOR non-lin and Rhino employs NNs to learn causal relationships, and the non-linearity in regime 1 complicates graph learning for the other models. CASTOR outperforms CD-NOD in this real world settings due to the fact that CD-NOD assumes that only few variables change from one regime to the other.

Table 2: F1 Scores across IT data.

Model	Graph type	F1 Reg1	F1 Reg 2
PCMCi+	W	12.1	29.6
DYNOTEARS	W	18.2	28.5
Rhino	W	28.6	25.8
CASTOR	W	18.2	28.5
CASTOR non-lin	W	40.0	24.5
CD-NOD	S		23.5
CASTOR non-lin	S		36.8

As it is evident from Table 2, CASTOR proficiently identifies the exact number of regimes and their indices. On regime 2, CASTOR (with linear relationships), PCMCi+ and DYNOTEARS outperform Rhino and CASTOR non-lin (uses NN for non linear relationships). However, in regime 1, CASTOR non-linear and Rhino outperform all other models. This superiority can be attributed to the fact that CASTOR non-lin and Rhino employs NNs to learn causal relationships, and the non-linearity in regime 1 complicates graph learning for the other models. CASTOR outperforms CD-NOD in this real world settings due to the fact that CD-NOD assumes that only few variables change from one regime to the other.

5.3 Biosphere–Atmosphere data

We apply CASTOR to Biosphere atmosphere data¹. The objective is to demonstrate the practical utility of CASTOR in a real-world scenario.

[21] employ this type of data to learn causal relations between six variables (global radiation (R_g), air temperature (T_{air}), net ecosystem exchange (NEE), vapor pressure deficit (VPD), sensible heat (H), latent heat flux (LE)) under climate change conditions. They utilize the causal discovery model PCMCi+ for windows of three months (with one overlapping month) to learn causal relations. The objective of our experiments is to automate the learning of causal graphs and regime partitions. In other words, instead of assuming that the causal graph changes every three months and applying a causal discovery method at that interval, we provide MTS of one year’s length to CASTOR and we let the model (CASTOR) decide when the causal graph changes and which months are more similar. Although we initially set a window length of three months, CASTOR stabilizes after a few iterations in a state with two regimes.

It is essential to note that assuming causal sufficiency in this setting is a difficult assumption, as the biosphere-atmosphere relationship is considerably more complex in reality. Consequently, validating

¹FLUXNET Dataset San Luis site, Argentina published by [11]

the causal sufficiency assumption is challenging, which explains the appearance of some suspicious relationships. Nevertheless, we will interpret some of the relations and explain why certain causal relations appear and why others are inverted.

In our application, we use CASTOR on this MTS data of six variables, aiming to automatically learn the regime partition and the causal graphs. Initiating with non-overlapping windows of three months (4 initialed different regimes) and a minimum regime duration of two months, CASTOR splits the data into two regimes: the first corresponds to the cold regime grouping Autumn and Winter (From April to September), while the second encompasses Summer and Spring. The accuracy of this partition is 85.4%, with some days in the second regime occasionally misclassified as the first one.

Regarding the causal links, an initial observation is that the strength (represented by thickness) of certain causal relations is greater in the hot regime (yellow) compared to the cold regime (blue). Furthermore, all variables in both regimes are identified as parents of global radiation, which is intuitively incorrect. However, this observation can be explained by our assumption of causal sufficiency, where we assume observation of all causal variables, which is, in reality, not accurate. To explain this result, our model interprets global radiation as the net radiation. Mathematically, we have:

$$R_n = R_g - SW_{\uparrow} + LW_{\downarrow} - LW_{\uparrow},$$

where R_n is the net radiation, R_g is the global radiation which is also global shortwave radiation, part of the the incoming radiation is reflected at the surface (shortwave upward radiation $SW_{\uparrow} = \alpha R_g$, LW_{\uparrow} is the long-wave upward radiation which is the amount of long-wave radiation emitted at the surface and LW_{\downarrow} is the long-wave downward radiation. Also we have that the net radiation R_n :

$$R_n = H + LE + G,$$

where H is the sensible heat, LE is the latent heat flux and G is the ground heat flux.

In our setting, where we assume causal sufficiency (which is not accurate), CASTOR learns incorrect link directions. Every variable appears to act as a parent of R_g (global radiation), a behavior explained by the two equations above, where CASTOR interprets R_g as the net radiation R_n . Additionally, we observe that temperature influences vapor pressure deficit (VPD), which is understandable. For instance, in hot weather, evaporation can be sustained for a longer period, leading to higher VPD (VPD is the difference between the maximum moisture that could be hold in the air could hold and the actual moisture in the air). Furthermore, we can notice that the temperature T_{air} is a common cause of sensible heat H and latent heat flux LE which is understandable as we know that these two variable can mathematically be described as function temperature. The relationship between NEE and LE is complex and influenced by various factors including plant physiology, climate, soil moisture, and atmospheric conditions. There’s no direct relation linking NEE and LE , both variables are influenced by the conductance of stomata which regulates both CO_2 uptake for photosynthesis (affecting NEE) and water vapor release (affecting LE). Thus, having this common confounder variable causes the appearance of suspicious link ($NEE \rightarrow LE$). As we mentioned, LE is affected by water vapor release, which mathematically could be written as follows: $LE \propto g_s \cdot VPD$ where (VDP) Vapor pressure deficit and g_s is the conductance of stomata. Hence, this equation explains the link $VPD \rightarrow LE$.

The key difference between the two regimes lies in the strength of the causal relationships. This is because the variables take on different values in each regime. This finding demonstrates CASTOR’s ability to distinguish between graphs with identical structures but varying edge weights.

6 Related works

Assad et al. [3] offer an extensive survey of methods for learning temporal causal relationships. Granger causality is the primary approach used for causal discovery from MTS [7, 24, 44]. However, it is unable to accommodate instantaneous effects. DYNOTEARS [27], on the other hand, leverages the acyclicity constraint established by [45] to continuously relax the DAG and differentially learn instantaneous and time lagged structures. However, DYNOTEARS is still limited to linear functional forms. TiMINo [30] provides a general theoretical framework for temporal causal discovery with functional causal models. However, the aforementioned methods assume that MTS are composed of a single regime.

Several studies have sought to tackle the challenge of causal discovery in heterogeneous data

[13, 16, 36, 37, 47]. Remarkably, [16] address heterogeneous time series by modulating causal relationships through a regime index. While it provides a summary graph highlighting behavioral changes across regimes, they cannot infer individual causal graphs neither the exact number of regime. Finally, [37] assume knowledge of the number of regimes and propose the inference of only time-lagged links. Furthermore, they evaluate their algorithm on graphs with a limited number of nodes (Detailed related work in Appendix A).

7 Conclusion

We introduce CASTOR, a framework designed to learn causal relationships from MTS composed of multiple regimes. As the first method to simultaneously learn the number of regimes, their indices, and infer causal graphs per regime, CASTOR outperforms causal discovery models in effectively handling both linear and non-linear relationships across multiple regimes in synthetic and real datasets.

Acknowledgements

We thank Ali Mourtada, Guillermo Ortiz-Jimenez, Nikolaos Dimitriadis, Anas Essounaini, Thibault Séjourné for helpful feedbacks and comments. This work was supported by the SNSF Sinergia project ‘PEDESITE: Personalized Detection of Epileptic Seizure in the Internet of Things (IoT) Era’

References

- [1] Ali Ait-Bachir, Charles K Assaad, Christophe de Bignicourt, Emilie Devijver, Simon Ferreira, Eric Gaussier, Hosein Mohanna, and Lei Zan. Case studies of causal discovery from it monitoring time series. *arXiv Preprint arXiv:2307.15678*, 2023. [9](#), [20](#)
- [2] Sylvain Arlot, Alain Celisse, and Zaid Harchaoui. A kernel multiple change-point algorithm via model selection. *Journal of machine learning research*, 2019. [9](#), [25](#)
- [3] Charles K Assaad, Emilie Devijver, and Eric Gaussier. Survey and evaluation of causal discovery methods for time series. *Journal of Artificial Intelligence Research*, 2022. [10](#), [16](#), [24](#)
- [4] Karim Assaad, Emilie Devijver, Eric Gaussier, and Ali Ait-Bachir. A mixed noise and constraint-based approach to causal inference in time series. In *ECML PKDD*, 2021. [17](#)
- [5] Albert-László Barabási and Réka Albert. Emergence of scaling in random networks. *Science*, 1999. [7](#), [20](#)
- [6] Philippe Brouillard, Sébastien Lachapelle, Alexandre Lacoste, Simon Lacoste-Julien, and Alexandre Drouin. Differentiable causal discovery from interventional data. In *Advances in Neural Information Processing Systems*, 2020. [6](#), [16](#)
- [7] Bart Bussmann, Jannes Nys, and Steven Latré. Neural additive vector autoregression models for causal discovery in time series. In *Discovery Science*, 2021. [1](#), [10](#)
- [8] Daria Bystrova, Charles K Assaad, Julyan Arbel, Emilie Devijver, Eric Gaussier, and Wilfried Thuiller. Causal discovery from time series with hybrids of constraint-based and noise-based algorithms. *arXiv e-prints*, pages arXiv–2306, 2023. [9](#)
- [9] Arthur P Dempster, Nan M Laird, and Donald B Rubin. Maximum likelihood from incomplete data via the em algorithm. *Journal of the royal statistical society*, 1977. [4](#)
- [10] Doris Entner and Patrik O Hoyer. On causal discovery from time series data using fci. *Probabilistic graphical models*, 2010. [16](#)
- [11] Alfredo Garcia, Carlos Bella, Javier Houspanossian, Patricio Magliano, Esteban Jobbágy, Gabriela Posse, Roberto Fernández, and Marcelo Nosetto. Fluxnet2015 ar-slu san luis, dataset(2009-2011). 2015. [9](#)
- [12] Wenbo Gong, Joel Jennings, Cheng Zhang, and Nick Pawlowski. Rhino: Deep causal temporal relationship learning with history-dependent noise. *Preprint arXiv:2210.14706*, 2022. [1](#), [2](#), [3](#), [8](#), [17](#), [21](#), [23](#), [28](#), [32](#)
- [13] Wiebke Günther, Urmi Ninad, and Jakob Runge. Causal discovery for time series from multiple datasets with latent contexts. *Preprint arXiv:2306.12896*, 2023. [11](#)
- [14] Uzma Hasan, Emam Hossain, and Md Osman Gani. A survey on causal discovery methods for iid and time series data. *Transactions on Machine Learning Research*, 2023. [16](#)
- [15] Stefan Haufe, Klaus-Robert Müller, Guido Nolte, and Nicole Krämer. Sparse causal discovery in multivariate time series. In *causality: objectives and assessment*, pages 97–106. PMLR, 2010. [16](#)
- [16] Biwei Huang, Kun Zhang, Jiji Zhang, Joseph Ramsey, Ruben Sanchez-Romero, Clark Glymour, and Bernhard Schölkopf. Causal discovery from heterogeneous/nonstationary data. *Journal of Machine Learning Research*, 21(1), 2020. [1](#), [2](#), [3](#), [4](#), [7](#), [9](#), [11](#), [17](#), [24](#), [25](#)

- [17] Antti Hyttinen, Frederick Eberhardt, and Matti Järvisalo. Constraint-based causal discovery: Conflict resolution with answer set programming. In *UAI*, pages 340–349, 2014. 16
- [18] Aapo Hyvärinen, Kun Zhang, Shohei Shimizu, and Patrik O Hoyer. Estimation of a structural vector autoregression model using non-gaussianity. *Journal of Machine Learning Research*, 11(5), 2010. 8, 16, 20, 21, 23
- [19] Soufiane Karmouche, Evgenia Galytska, Jakob Runge, Gerald A Meehl, Adam S Phillips, Katja Weigel, and Veronika Eyring. Regime-oriented causal model evaluation of atlantic–pacific teleconnections in cmip6. *Earth System Dynamics*, 2023. 1
- [20] Nan Rosemary Ke, Olexa Bilaniuk, Anirudh Goyal, Stefan Bauer, Hugo Larochelle, Bernhard Schölkopf, Michael C Mozer, Chris Pal, and Yoshua Bengio. Learning neural causal models from unknown interventions. *Preprint arXiv:1910.01075*, 2019. 16
- [21] Christopher Krich, Mirco Migliavacca, Diego G Miralles, Guido Kraemer, Tarek S El-Madany, Markus Reichstein, Jakob Runge, and Miguel D Mahecha. Functional convergence of biosphere–atmosphere interactions in response to meteorological conditions. *Biogeosciences*, 2021. 9
- [22] Chenxi Liu and Kun Kuang. Causal structure learning for latent intervened non-stationary data. In *International Conference on Machine Learning*, 2023. 1, 6
- [23] Lars Lorch, Jonas Rothfuss, Bernhard Schölkopf, and Andreas Krause. Dibs: Differentiable bayesian structure learning. In *Advances in Neural Information Processing Systems*, 34:24111–24123, 2021. 16
- [24] Sindy Löwe, David Madras, Richard Zemel, and Max Welling. Amortized causal discovery: Learning to infer causal graphs from time-series data. In *Conference on Causal Learning and Reasoning*, 2022. 1, 10
- [25] Raha Moraffah, Paras Sheth, Mansooreh Karami, Anchit Bhattacharya, Qianru Wang, Anique Tahir, Adrienne Raglin, and Huan Liu. Causal inference for time series analysis: Problems, methods and evaluation. *Knowledge and Information Systems*, 63:3041–3085, 2021. 1
- [26] Mark Newman. *Networks*. Oxford university press, 2018. 7, 20
- [27] Roxana Pamfil, Nisara Sriwattanaworachai, Shaan Desai, Philip Pilgerstorfer, Konstantinos Georgatzis, Paul Beaumont, and Bryon Aragam. Dynotears: Structure learning from time-series data. In *International Conference on Artificial Intelligence and Statistics*, 2020. 1, 2, 3, 4, 6, 8, 10, 16, 20, 23
- [28] Jonas Peters and Peter Bühlmann. Identifiability of gaussian structural equation models with equal error variances. *Biometrika*, 101(1):219–228, 2014. 4, 7, 32
- [29] Jonas Peters, Joris Mooij, Dominik Janzing, and Bernhard Schölkopf. Identifiability of causal graphs using functional models. *Preprint arXiv:1202.3757*, 2012. 7, 32
- [30] Jonas Peters, Dominik Janzing, and Bernhard Schölkopf. Causal inference on time series using restricted structural equation models. In *Advances in Neural Information Processing Systems*, 2013. 10, 16, 32
- [31] Jonas Peters, Dominik Janzing, and Bernhard Schölkopf. *Elements of causal inference: foundations and learning algorithms*. The MIT Press, 2017. 28, 32
- [32] Abdellah Rahmani, Arun Venkitaraman, and Pascal Frossard. A meta-gnn approach to personalized seizure detection and classification. In *IEEE International Conference on Acoustics, Speech and Signal Processing (ICASSP)*, 2023. 1
- [33] Jakob Runge. Causal network reconstruction from time series: From theoretical assumptions to practical estimation. *Chaos: An Interdisciplinary Journal of Nonlinear Science*, 28(7), 2018. 1, 28
- [34] Jakob Runge. Discovering contemporaneous and lagged causal relations in autocorrelated nonlinear time series datasets. In *Conference on Uncertainty in Artificial Intelligence*, pages 1388–1397. PMLR, 2020. 2, 8, 16, 20, 21, 23

- [35] Jakob Runge, Peer Nowack, Marlene Kretschmer, Seth Flaxman, and Dino Sejdinovic. Detecting and quantifying causal associations in large nonlinear time series datasets. *Science advances*, 2019. 1, 16
- [36] Basil Saeed, Snigdha Panigrahi, and Caroline Uhler. Causal structure discovery from distributions arising from mixtures of dags. In *International Conference on Machine Learning*, 2020. 11
- [37] Elena Saggioro, Jana de Wiljes, Marlene Kretschmer, and Jakob Runge. Reconstructing regime-dependent causal relationships from observational time series. *Chaos: An Interdisciplinary Journal of Nonlinear Science*, 30(11), 2020. 1, 2, 7, 11, 17, 20, 21
- [38] Xinpeng Shen, Sisi Ma, Prashanthi Vemuri, and Gyorgy Simon. Challenges and opportunities with causal discovery algorithms: application to alzheimer’s pathophysiology. *Scientific reports*, 2020. 1
- [39] Le Song, Mladen Kolar, and Eric Xing. Time-varying dynamic bayesian networks. In *Advances in Neural Information Processing Systems*, 22, 2009. 16
- [40] Peter Spirtes, Clark N Glymour, Richard Scheines, and David Heckerman. *Causation, prediction, and search*. MIT press, 2000. 16
- [41] Siyi Tang, Jared A Dunnmon, Khaled Saab, Xuan Zhang, Qianying Huang, Florian Dubost, Daniel L Rubin, and Christopher Lee-Messer. Self-supervised graph neural networks for improved electroencephalographic seizure analysis. *Preprint arXiv:2104.08336*, 2021. 1
- [42] Sofia Triantafillou and Ioannis Tsamardinos. Constraint-based causal discovery from multiple interventions over overlapping variable sets. *The Journal of Machine Learning Research*, 16(1): 2147–2205, 2015. 16
- [43] Tailin Wu, Thomas Breuel, Michael Skuhersky, and Jan Kautz. Discovering nonlinear relations with minimum predictive information regularization. *Preprint arXiv:2001.01885*, 2020. 1
- [44] Chenxiao Xu, Hao Huang, and Shinjae Yoo. Scalable causal graph learning through a deep neural network. In *ACM international conference on information and knowledge management*, 2019. 10
- [45] Xun Zheng, Bryon Aragam, Pradeep K Ravikumar, and Eric P Xing. Dags with no tears: Continuous optimization for structure learning. In *Advances in neural information processing systems*, 2018. 6, 10, 16
- [46] Xun Zheng, Chen Dan, Bryon Aragam, Pradeep Ravikumar, and Eric Xing. Learning sparse nonparametric dags. In *International Conference on Artificial Intelligence and Statistics*, 2020. 6
- [47] Fangting Zhou, Kejun He, and Yang Ni. Causal discovery with heterogeneous observational data. In *Uncertainty in Artificial Intelligence*, 2022. 11
- [48] Ciyu Zhu, Richard H Byrd, Peihuang Lu, and Jorge Nocedal. Algorithm 778: L-bfgs-b: Fortran subroutines for large-scale bound-constrained optimization. *ACM Transactions on mathematical software (TOMS)*, 1997. 21
- [49] Shengyu Zhu, Ignavier Ng, and Zhitang Chen. Causal discovery with reinforcement learning. *Preprint arXiv:1906.04477*, 2019. 16

Appendix organization:

A Detailed related work	16
B Illustrative figures of CASTOR framework	17
C Limitation and broader impact	18
D Expectation-Maximization derivation	19
E Further experimental results	20
E.1 Synthetic data	20
E.2 Web activity data	20
E.3 Baselines	20
E.4 Further experiments and evaluation using SHD: Linear case	21
E.5 Further experiments and evaluation using SHD: nonlinear case	22
E.6 Further experiments: Comparison with CD-NOD	24
E.7 Further experiments: Regime detection experiment	25
E.8 Models running time	26
F Regime and causal graphs identifiability	28
F.1 Proof of theorem 1	29
F.1.1 Optimizing the score will lead to pure regimes	30
F.1.2 In case of edge disagreement $\mathcal{S}(\mathcal{G}^*, \mathcal{E}^*) > \mathcal{S}(\hat{\mathcal{G}}, \hat{\mathcal{E}})$	32
F.2 Proof of theorem 4.2	33
G Illustration of CASTOR’s estimated graphs	36
G.1 Illustration of the estimated graphs by CASTOR: Linear case, 5 regimes with $L = 1$	36
G.2 Illustration of the estimated graphs by CASTOR: Linear case, 2 regimes with $L = 2$	37
G.3 Illustration of the estimated graphs by CASTOR: Non-linear case, 3 regimes with $L = 1$	38
G.4 Illustration of the estimated graphs by CASTOR: Non-linear case, 5 regimes with $L = 1$	39

Algorithm 1 CASTOR algorithm

Input: MTS \mathbf{X} , window size W , lag L , maximum number of iteration N_{iter} , minimum regime duration ζ
for $i = 1$ **to** N_{iter} **do**
 $\gamma_{t,u} \leftarrow \frac{\pi_{t,u}(\alpha) f^u(\mathbf{x}_t)}{\sum_{j=1}^{N_w} \pi_{t,j}(\alpha) f^j(\mathbf{x}_t)}$
 $\alpha \leftarrow \operatorname{argmin}_{\alpha} \sum_{u=1}^K \sum_{t=1}^{|\mathcal{T}|} \gamma_{t,u} \log(\pi_{t,u}(\alpha))$
 $\mathcal{G} \leftarrow \operatorname{argmin}_{\alpha}$ of Eq (8) or (3.4)
 if $\sum_t^{|\mathcal{T}|} \gamma_{t,u} \leq \zeta$ **then**
 $\forall t : \gamma_{t,u} \leftarrow 0$
 end if
end for
Output: γ, \mathcal{G}

A Detailed related work

Causal structure learning has been a hot research topics, [14] propose a survey on causal discovery from IID data and time series. For IID data, Some approaches rely on conditional independence to infer causal relationships from observational data. A classic example of such approach is the PC algorithm [40]. In addition to approaches that work with observational data, there are also methods that support interventional data (COMBINE [42] and HEJ [17]). These methods offer insights into causal relationships based on data acquired through controlled interventions.

A novel line of research introduced by [45] has sought to address the combinatorial problem of structure learning by formulating it as a continuous constrained optimization problem. By adopting this approach, they successfully circumvent the need for computationally intensive combinatorial search methods. Similarly, [49] leverage the acyclicity constraint in their work but employ reinforcement learning techniques as a search strategy to estimate the DAG. In contrast, [20] focus on learning a DAG from interventional data through the optimization of an unconstrained objective function. [6] have undertaken a comprehensive investigation into the application of continuous-constrained approaches in the context of interventions, providing a general framework for their utilization. Another notable approach, DiBS by [23], aims to infer a full posterior distribution over Bayesian networks given limited available observations. This approach enables the quantification of the uncertainty and the estimation of confidence levels of the structure learning procedure.

The aforementioned state-of-the-art methods have primarily been applied in the context of independent observations over time. [3] offer an extensive survey for learning temporal causal relationships. However, when it comes to modeling time-dependent causal relationships, researchers have introduced and utilized Dynamic Bayesian Networks (DBNs). DBNs allow for the modeling of discrete-time temporal dynamics within directed graphical models. In certain approaches, contemporaneous dependencies are disregarded, and the focus is solely on recovering time-lagged relationships. Examples of such approaches include the works of [15], [39], and the algorithm tsFCI [10] adapts the Fast Causal Inference [40] algorithm (developed for the causal analysis of non-temporal variables) to infer causal relationships from time series data. [35] proposed a two-stage algorithm PCMCI that can scale to large time series. However, these methods primarily emphasize the identification of relationships between variables at different time points, without explicitly considering contemporaneous relationships. [34] present an extension of PCMCI called PCMCI+ that learns contemporary or instantaneous causal links. Another line of research targets the model with non-Gaussian instantaneous models, [18] propose, VARLINGAM, a model that combines the non-Gaussian instantaneous models with autoregressive models and shows that a non-Gaussian model is identifiable without prior knowledge of network structure. Another approach, called Time-series Models with Independent Noise (TiMINo) [30] studies a class of restricted structural equation models (SEMs) for time-series data that include nonlinear and instantaneous effects. Recently, a novel study conducted by [27] has emerged, utilizing the algebraic characterization of acyclicity in directed graphs established by [45]. Their work focuses on the learning of instantaneous and time-lagged graphs within time series data. To achieve this, they have developed a score-based approach for learning DBNs and employed an augmented lagrangian to optimize the resulting program. The resultant method, known as DYNOTEARS, offers the

ability to learn causal graph of time dependent variable, without making implicit assumptions about the underlying graph topologies. By leveraging the algebraic characterization of acyclicity, DYNOTEARS enables the estimation of both instantaneous and time-lagged relationships in time series data. Instead of learning a full temporal causal graph, some methods like NBCB [4] or Noise-based/Constraint-based approach learns a summary causal graph from observational time series data without being restricted to the Markov equivalent class even in the case of instantaneous relations.

While DYNOTEARS, Rhino [12], PCMCI+, VARLINGAM successfully learn both instantaneous and time-lagged relationships from time series data, it is important to note that the method assumes stationarity and a single regime for the data. However, in numerous real-world scenarios, time series data may exhibit non-stationarity or be composed of multiple regimes, where the causal relationships are different in each regime. This presents a significant challenge for causal discovery. Some research have aimed to address this challenge by developing methods for causal discovery in heterogeneous data. An example of such a method is CD-NOD developed by [16], tackles time series with various regimes. By using the time stamp IDs as a surrogate variable, CD-NOD output one summary causal graph where the parents of each variable are identified as the union of all its parents in graphs from different regimes. Then it detects the change points by using a non stationary driving force that estimates the variability of the conditional distribution $p(x_i|\text{union parents of } x_i)$ over the time index surrogate. While CD-NOD provides a summary graph capturing behavioral changes across regimes, it falls short in inferring individual causal graphs. The overall summary graph does not effectively highlight changes between regimes. Additionally, CD-NOD detects the change points but fails to determine the regime indices, rendering it incapable of inferring the precise number of regimes. In scenarios involving recurring regimes, CD-NOD is unable to detect this crucial information. Another relevant work dealing with MTS composed of multiple regimes is RPCMCI [37]. In this approach, [37] learn a temporal graph for each regime. However, they focus initially on inferring only time-lagged relationships and require prior knowledge of the number of regimes and transitions between them.

B Illustrative figures of CASTOR framework

CASTOR represents a causal discovery framework tailored for Multivariate Time Series (MTS), composed of different regimes. Each regimes can be treated as an independent MTS. Additionally, it is crucial to note that the number of lags L always remains below the minimum length of the regimes ζ .

Figure (7) illustrates a MTS on its left side comprising three variables and two unknown distinct regimes. Each regime possesses its temporal DAG, with one lag attributed to each in this demonstrative scenario.

Upon receiving the MTS as input, CASTOR engages in the process of discerning the number of regimes, determining the indices associated with each regime (indicating their commencement and conclusion), and inferring the temporal DAGs. The resultant DAGs facilitate the straightforward reconstruction of summary graphs encapsulating the entire MTS (CD-NOD output).

To elucidate the regime learning process, Figure (8) delineates the step-by-step procedure followed by CASTOR in determining the number of regimes and their corresponding indices. The process commences with CASTOR partitioning the MTS into equal windows. In the initial iteration, the length of each regime equals the window size, a user-specified hyperparameter.

Subsequently, CASTOR learns a temporal DAG for each regime. This involves solving an optimization problem, as outlined in Eq (8) for the linear case and Eq (3.4) for the non-linear scenario. Following graph acquisition, CASTOR updates the regime indices utilizing Eq (6). Notably, CASTOR employs a filtering mechanism to eliminate regimes characterized by an insufficient number of samples. In practical terms, any regime with fewer samples than a defined hyperparameter, denoted as ζ (representing the minimum regime duration), is discarded.

In the event of regime elimination, samples from the discarded regimes are reallocated to the nearest regime in terms of probability. Specifically, if the discarded regime is denoted as u , the sample x_t will be assigned to regime v in the subsequent iteration, where v is the regime with the highest $\gamma_{t,v}$.

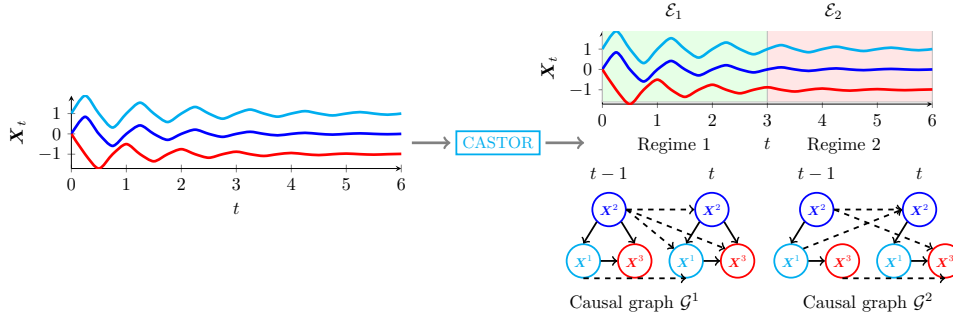


Figure 7: Overview of CASTOR: This illustration demonstrates that CASTOR relies on the MTS to infer the number of regimes (equal to 2 in this figure), the regime partition (\mathcal{E}_1 for the first regime and \mathcal{E}_2 for the second) and learn the temporal causal graphs (\mathcal{G}^1 for the first regime and \mathcal{G}^2 for the second). Dashed edges symbolize time-lagged links, while normal arrows represent instantaneous links.

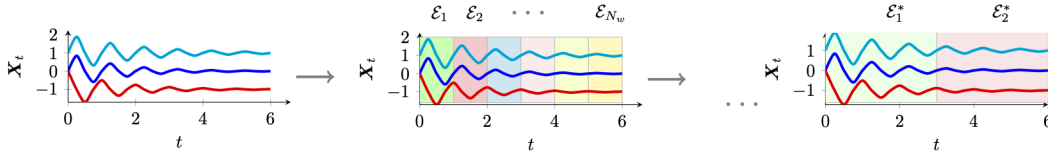


Figure 8: CASTOR initially starts with N_w equal windows, employing the M-step to learn the graph for the initial regimes. The method alternates between updating regime indices in the E-step and inferring temporal causal graphs in the M-step until maximum iterations. Over iterations, some initial regimes disappear, resulting in N_w gradually approaching K (two in this figure).

C Limitation and broader impact

Limitation. A fundamental limitation of this work is the assumption that the noises are Gaussian. Future research could address this by extending the analysis to non-Gaussian noise models. Another valuable direction would be to conduct a statistical analysis to understand how the number of samples affects the performance of CASTOR in each regime. Additionally, extending the framework to account for the presence of confounders represents an important avenue for future work.

Broader impact. This work proposes a theoretical analysis and technical methods to learn the number of regimes, their indices and temporal causal graphs from time-series data composed of multiple regime, which facilitate the construction of more transparent and interpretable models to understand the causal effect in the real world. This could be beneficial in a variety of sectors, including healthcare, finance, and technology. In contrast, misinterpretations of causal relationships could also have significant negative implications in these fields, which must be carefully done to avoid unfair or biased predictions.

D Expectation-Maximization derivation

In this section, we shall elucidate the computational details surrounding the resolution of our optimization problem. Specifically, we will provide clarity on the various equations introduced in Section 3, namely, Eq (7, 8, 6, 3.4).

E-step. We model regime participation through a binary latent variable $z_t \in \mathbf{R}^{N_w}$; \mathbf{x}_t belongs to regime $u \Rightarrow z_{t,u} = 1$.

$$\begin{aligned} \gamma_{t,u} &= p\left(z_{t,u} = 1 \mid \mathbf{x}_t, \mathbf{x}_{<t}, \mathbf{G}_{\{0:L\}}^u\right) \\ &= \frac{p(z_{t,u} = 1) p\left(\mathbf{x}_t \mid \mathbf{x}_{<t}, z_{t,u} = 1, \mathbf{G}_{\{0:L\}}^u\right)}{\sum_{j=1}^{N_w} p(z_{t,j} = 1) p\left(\mathbf{x}_t \mid \mathbf{x}_{<t}, z_{t,j} = 1, \mathbf{G}_{\{0:L\}}^j\right)} \\ &= \frac{\pi_{t,u}(\alpha) f^u(\mathbf{x}_t)}{\sum_{j=1}^{N_w} \pi_{t,j}(\alpha) f^j(\mathbf{x}_t)} \end{aligned} \quad (1)$$

M-step. Having estimated probabilities $\gamma_{t,u}$ in the E-step, we can now maximise the expected posterior distribution given the MTS $(\mathbf{x}_t)_{t \in \mathcal{T}}$ and we have:

$$\begin{aligned} &\sup_{\theta, \alpha} \frac{1}{|\mathcal{T}|} \sum_{u=1}^{N_w} \sum_{t=0}^{|\mathcal{T}|} \gamma_{t,u} \log \pi_{t,u}(\alpha) f^u(\mathbf{x}_t) - \lambda |\mathcal{G}^u|, \text{ s.t } \mathbf{G}_0^u \text{ is a DAG,} \\ &\iff \begin{cases} \max_{\alpha} \frac{1}{|\mathcal{T}|} \sum_{u=1}^{N_w} \sum_{t=1}^{|\mathcal{T}|} \gamma_{t,u} \ln(\pi_{t,u}(\alpha)) \\ \sup_{\theta} \frac{1}{|\mathcal{T}|} \sum_{u=1}^{N_w} \sum_{t \in \mathcal{E}_u} \log f^u(\mathbf{x}_t) - \lambda |\mathcal{G}^u|, \text{ s.t } \mathbf{G}_0^u \text{ is a DAG,} \end{cases} \end{aligned} \quad (2)$$

We know $f^u(\mathbf{x}_t) = \mathcal{N}\left(\mathbf{x}_t \mathbf{G}_0^u + \sum_{\tau=1}^L \mathbf{x}_{t-\tau} \mathbf{G}_{\tau}^u, I\right)$, hence:

$$\begin{aligned} &\iff \sup_{\theta} \frac{1}{|\mathcal{T}|} \sum_{u=1}^{N_w} \sum_{t \in \mathcal{E}_u} \log f^u(\mathbf{x}_t) - \lambda |\mathcal{G}^u|, \text{ s.t } \mathbf{G}_0^u \text{ is a DAG,} \\ &\iff \min_{\theta} \frac{1}{|\mathcal{T}|} \sum_{u=1}^{N_w} \sum_{t \in \mathcal{E}_u} \left\| \mathbf{x}_t - \left(\mathbf{x}_t \mathbf{G}_0^u + \sum_{\tau=1}^L \mathbf{x}_{t-\tau} \mathbf{G}_{\tau}^u \right) \right\|_F^2 + \lambda |\mathcal{G}^u|, \text{ s.t } \mathbf{G}_0^u \text{ is a DAG} \\ &\iff \min_{\theta} \frac{1}{|\mathcal{T}|} \sum_{u=1}^{N_w} \sum_{t=1}^{|\mathcal{T}|} \gamma_{t,u} \left\| \mathbf{x}_t - \left(\mathbf{x}_t \mathbf{G}_0^u + \sum_{\tau=1}^L \mathbf{x}_{t-\tau} \mathbf{G}_{\tau}^u \right) \right\|_F^2 + \lambda |\mathcal{G}^u|, \text{ s.t } \mathbf{G}_0^u \text{ is a DAG} \\ &\iff \min_{\theta} \frac{1}{|\mathcal{T}|} \sum_{u=1}^{N_w} \sum_{t=1}^{|\mathcal{T}|} \gamma_{t,u} \left\| \mathbf{x}_t - \left(\mathbf{x}_t \mathbf{G}_0^u + \sum_{\tau=1}^L \mathbf{x}_{t-\tau} \mathbf{G}_{\tau}^u \right) \right\|_F^2 + \lambda |\mathcal{G}^u| + \frac{\rho}{2} h(\mathbf{G}_0^u)^2 + \alpha h(\mathbf{G}_0^u), \end{aligned} \quad (3)$$

The only difference between the linear and the non linear cases is how we estimate the mean of the normal distribution f^u for every regime u . As we mentioned in section 3.2, we estimate these means using NNs and we have $f_i^u(\mathbf{x}_t) = \mathcal{N}\left(\psi_i^u\left(\phi_i^u(\mathbf{x}_t), \phi_i^{u,\text{lag}}(\mathbf{x}_t^{\text{lag}})\right), 1\right)$, Hence, our M-step for non-linear CASTOR:

$$\min_{\theta, \mathcal{G}} \frac{1}{|\mathcal{T}|} \sum_{u=1}^{N_w} \sum_{t=1}^{|\mathcal{T}|} \sum_{i=1}^d \gamma_{t,u} \mathcal{L}(x_t^i, \psi_i^u\left(\phi_i^u(\mathbf{x}_t), \phi_i^{u,\text{lag}}(\mathbf{x}_t^{\text{lag}})\right)) + \lambda |\mathcal{G}^u| + \frac{\rho}{2} h(\mathbf{G}_0^u)^2 + \alpha h(\mathbf{G}_0^u) \quad (4)$$

E Further experimental results

E.1 Synthetic data

We employ the Erdos–Rényi (ER) [26] model with mean degrees of 1 or 2 to generate lagged graphs, and the Barabasi–Albert (BA) [5] model with mean degrees 4 for instantaneous graphs. The maximum number of lags, L , is set at 1 or 2. We experiment with varying numbers of nodes $\{5, 10, 20, 40\}$ and different numbers of regimes $\{2, 3, 4, 5\}$, each representing diverse causal graphs. The length of each regime is randomly sampled from the set $\{300, 400, 500, 600\}$.

- **Linear case.** Data is generated as follows:

$$\forall u \in \{1, \dots, K\}, \forall t \in \mathcal{E}_u : \mathbf{x}_t = \mathbf{x}_t \mathbf{G}_0^u + \sum_{\tau=1}^L \mathbf{x}_{t-\tau} \mathbf{G}_\tau^u + \epsilon_t,$$

with \mathbf{G}_0^u is adjacency matrix of the generated graph by BA model, $\forall \tau \in \{1, \dots, L\} : \mathbf{G}_\tau^u$ are the adjacency of the time lagged graphs generated by ER and $\epsilon_t \sim \mathcal{N}(0, I)$, follows to a normal distribution.

- **Non-linear case.** The formulation used to generated the data is:

$$\forall u \in \{1, \dots, K\}, \forall t \in \mathcal{E}_u : x_t^i = g_i^u(\mathbf{Pa}_{\mathcal{G}^u}^i(< t), \mathbf{Pa}_{\mathcal{G}^u}^i(t)) + \epsilon_t^i,$$

where g_i^u is a general differentiable linear/non-linear function and $\epsilon_t^i \sim \mathcal{N}(0, 1)$, follows a normal distribution. The function g_i^u is a random combination between a linear transformation and a randomly chosen function from the set: $\{\text{Tanh}, \text{LeakyReLU}, \text{ReLU}\}$.

E.2 Web activity data

The web activity dataset² has the following variables: NetIn that represents the data received by the network interface card in Kbytes/second; NPH represents the number of HTTP processes; NPP represents the number of PHP processes; NCM represents the number of open MySQL connections which are started by PHP processes, CpuH represents the percentage of CPU used by all HTTP processes; CpuP represents the percentage of CPU used by all PHP processes; CpuG represents the percentage of global CPU usage.

This dataset is challenging because it is collected from multiple sources resulting in a misaligned time series. Also the presence of partially sleeping time series (NetIn and NPP) due to inactivity of certain servers. The low sampling rate and also the presence of missing values (CpuG) can complicate the inference of causal relationships. Also, the experts in the field of IT systems are uncertain whether IT data, such as web activity data, satisfy the causal sufficiency assumption.

[1] presented a study about the challenges presented by IT monitoring time series, their results shows that the causal discovery method suffers in these scenarios due to aforementioned challenges.

E.3 Baselines

All used benchmarks for the synthetic experiments are run by using publicly available libraries: VARLINGAM [18] is implemented in the `lingam`³ python package. PCMCi+ [34] and RPCMCi [37] are implemented in `Tigramite`⁴ and `DYNOTEARS` [27] on `causalnex`⁵ package. For Rhino we use the publicly available GitHub shared by the authors⁶. We fine tuned the parameters to achieve the optimal graph for each model.

For CASTOR, an edge threshold of 0.4 is selected. In the linear scenario, we establish $\zeta = 100$ as the minimum regime duration, while in the non-linear context, ζ is set at 200. To demonstrate the

²https://github.com/ckassaad/causal_discovery_for_time_series

³<https://lingam.readthedocs.io/en/latest/>

⁴<https://jakobrunge.github.io/tigramite/>

⁵<https://causalnex.readthedocs.io/en/latest/>

⁶<https://github.com/microsoft/causica/tree/v0.0.0>

model’s robustness to the choice of the window size, we train CASTOR using diverse window sizes, specifically $w = 200$ or $w = 300$. For the sparsity coefficient, we use $\lambda = 0.05$. In order to optimise our M-step, we use L-BFGS-B algorithm [48].

E.4 Further experiments and evaluation using SHD: Linear case

Table 1: We report the average F1 Score on regimes for different Models and Settings for linear causal relationships: d denotes the number of nodes, K indicates the number of regimes, “ Split ” specifies whether the algorithm automatically splits the regimes (“ A ”) or if the split was done manually beforehand (“ M ”) for the models. And “ Graph type ” categorizes the type of returned graph as either window graph (“ W ”) or summary graph (“ S ”). Inst. refers to instantaneous links and Lag to time lagged edges.

Model	Split	Graph type	$d = 10$						$d = 40$					
			$K = 2$		$K = 3$		$K = 4$		$K = 2$		$K = 3$		$K = 4$	
			Inst.	Lag	Inst.	Lag	Inst.	Lag	Inst.	Lag	Inst.	Lag	Inst.	Lag
Rhino	M	W	22	25	35	43	53	60	136	372	199	539	265	693
Rhino w/o hist	M	W	5	14	9	28	11	32	136	189	208	340	273	420
PCMCI+	M	W	16	9	18	11	24	17	29	8	53	8	72	12
DYNOTEARS	M	W	<u>0</u>	<u>0</u>	<u>3</u>	<u>0</u>	1	1	0	<u>0</u>	<u>11</u>	<u>6</u>	<u>9</u>	<u>4</u>
RPCMCI	A	W	-	38	-	48	-	-	-	155	-	451	-	-
CASTOR	A	W	0	0	1	0	1	<u>2</u>	<u>2</u>	0	9	1	7	2

The evaluation using the SHD metric demonstrates consistent findings: CASTOR outperforms the baselines (Rhino, PCMCI+) even when we place these baselines in more favorable scenarios by providing them with the ground truth regime partition.

RPCMCI encounters challenges in our settings due to its assumption of only inferring time-lagged relations. This assumption makes our scenario more complex for this algorithm, impacting both regime learning and graph inference tasks.

Although our settings are identifiable, PCMCI+ infers a Markov equivalent class for the instantaneous links, which explains its performance deterioration, particularly in instantaneous relations.

Rhino, which is a state-of-the-art causal discovery method for nonlinear relationships, faces challenges in the absence of historical dependent noises (as confirmed by Figure 4 on page 24 of the Rhino paper). Moreover, Rhino utilizes ConvertibleGNN with Normalizing flows to learn the causal graphs. To train this model, a minimum of 50 time series of length 200 (10000 samples), all sharing the same causal graph. In contrast, our dataset consists of regimes that do not exceed 600 samples. This difference in dataset characteristics poses challenges for Rhino’s performance in our scenario.

Table 2: We report the average F1 Score on regimes for different Models and Settings for linear causal relationships: d denotes the number of nodes, K indicates the number of regimes, “ Split ” specifies whether the algorithm automatically splits the regimes (“ A ”) or if the split was done manually beforehand (“ M ”) for the models. And “ Graph type ” categorizes the type of returned graph as either window graph (“ W ”) or summary graph (“ S ”). Inst. refers to instantaneous links and Lag to time lagged edges.

Model	Split	Graph type	$d = 10$						$d = 40$					
			$K = 2$		$K = 3$		$K = 4$		$K = 2$		$K = 3$		$K = 4$	
			Inst.	Lag	Inst.	Lag	Inst.	Lag	Inst.	Lag	Inst.	Lag	Inst.	Lag
VARLINGAM	M	W	22.9 \pm 5.6	8.01 \pm 12	18.4 \pm 3.6	15.9 \pm 4.2	24.1 \pm 6.5	8.20 \pm 6.5	8.83 \pm 1.7	2.96 \pm 0.2	10.3 \pm 2.4	1.66 \pm 1.2	14.0 \pm 2.4	2.30 \pm 0.7
PCMCI+	M	W	98.5 \pm 2.1	86.1 \pm 11.1	99.0 \pm 1.4	88.6 \pm 9.4	96.2 \pm 1.8	85.9 \pm 6.9	59.2 \pm 2.9	79.8 \pm 5.1	61.5 \pm 1.4	81.9 \pm 5.1	60.2 \pm 4.0	81.4 \pm 3.6
RPCMCI	A	W	-	-	-	-	-	-	46.6 \pm 9.1	-	14.1 \pm 2.3	-	-	
CASTOR	A	W	100 \pm 0.0	100 \pm 0.0	100 \pm 0.0	100 \pm 0.0	97.3 \pm 1.9	97.2 \pm 2.0	97.0 \pm 2.7	100 \pm 0.0	88.1 \pm 6.2	89.9 \pm 5.1	98.3 \pm 1.4	99.7 \pm 0.4

We examine varying numbers of nodes, specifically $\{5, 20\}$, and generated time series with different regime counts $\{2, 3, 4\}$. Our model’s performance is benchmarked against multiple baselines, namely Rhino [12], PCMCI+ [34], RPCMCI [37] and VARLINGAM [18] and the results are presented in Table 2.

RPCMCI represents the sole baseline tailored to address a similar setting. RPCMCI necessitates prior knowledge of the number of regimes and the maximum number of transitions, and with this input, it only infers time-lagged relations. Even with this detailed information, RPCMCI struggles to achieve convergence, particularly in settings with more than 3 different regimes. The absence of the inference of instantaneous relationships in RPCMCI poses a challenge for learning regime indices within our setting, as we assume the presence of instantaneous relationships. In contrast, CASTOR does not only surpass RPCMCI in performance but also converges consistently, correctly identifying the number of regimes and recovering both the regime indices and the underlying causal graphs of each regime. We can notice that CASTOR successively infers the regime indices and learns as well the instantaneous links as well as time lagged relations.

When we compare CASTOR and PCMCI+ with VARLINGAM and Rhino. CASTOR and PCMCI+ also demonstrate markedly superior performance (Specially for $d = 5$ for PCMCI+, the model struggles when the number of nodes become greater). To provide context, we manually partition our generated data into K regimes to facilitate the evaluation of VARLINGAM, PCMCI+. We then execute these aforementioned models on each segmented regime, infer the graphs, and compare these composite structures against their true counterparts. Even when executing VARLINGAM, PCMCI+ separately on each regime, CASTOR still outperforms these models without access to any prior information, such as the number of regimes or the indices of the regimes. PCMCI+, while excelling in capturing time-lagged relations, faces challenges with instantaneous links, particularly when dealing with a higher number of nodes. It can only identify the graph up to MECs without explicit functional relations.

$K = 5$				
d	Method	Type	SHD	F1
10	VARLINGAM	Inst.	59	11.7 \pm 2.3
		Lag	51	4.69 \pm 2.4
	RPCMCI	Inst.	-	-
		Lag	-	-
	CASTOR	Inst.	4	98.4 \pm 1.4
		Lag	1	97.1 \pm 1.4

Table 3: F1 and SHD Scores by Models and Settings: d indicates number of nodes, K refers to the number of regimes, and 'Type' refers to the causal links as either instantaneous or time-lagged.

E.5 Further experiments and evaluation using SHD: nonlinear case

Table 4: We report the SHD on regimes for different Models and Settings for linear causal relationships: d denotes the number of nodes, K indicates the number of regimes, " Split " specifies whether the algorithm automatically splits the regimes (" A ") or if the split was done manually beforehand (" M ") for the models. And " Graph type " categorizes the type of returned graph as either window graph (" W ") or summary graph (" S "). Inst. refers to instantaneous links and Lag to time lagged edges.

Model	Split	Graph type	$d = 10$				$d = 40$			
			$K = 2$		$K = 4$		$K = 2$		$K = 4$	
			Inst.	Lag	Inst.	Lag	Inst.	Lag	Inst.	Lag
Rhino	M	W	21	29	43	53	71	106	128	207
Rhino w/o hist	M	W	<u>15</u>	10	<u>32</u>	7	57	10	123	<u>30</u>
PCMCI+	M	W	19	6	36	<u>17</u>	<u>49</u>	6	<u>91</u>	13
DYNOTEARS	M	W	16	6	42	16	57	31	99	47
CASTOR	A	W	3	6	27	22	18	<u>7</u>	58	33

In the SHD evaluation for non-linear settings, it's evident that CASTOR outperforms all the baselines in predicting instantaneous links. However, when it comes to time-lagged relationships, PCMCI+

excels and outperforms CASTOR. It’s important to highlight that PCMCI+ operates in a more favorable scenario, as it is provided with ground truth regime partitions. Nevertheless, CASTOR stands out for its ability to learn the graphs, determine the number of regimes, and identify their respective indices.

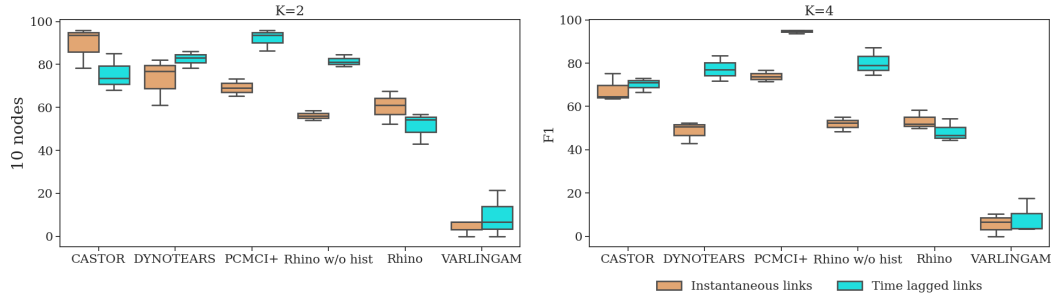


Figure 9: F1 scores by Models and Settings: Orange indicates performance on instantaneous links, and sky-blue signifies performance on time-lagged relationships. Notably, **CASTOR is the only model capable of learning the number of regimes and regime indices; for other baselines, a manual split was performed beforehand.** Number of nodes is 10 nodes

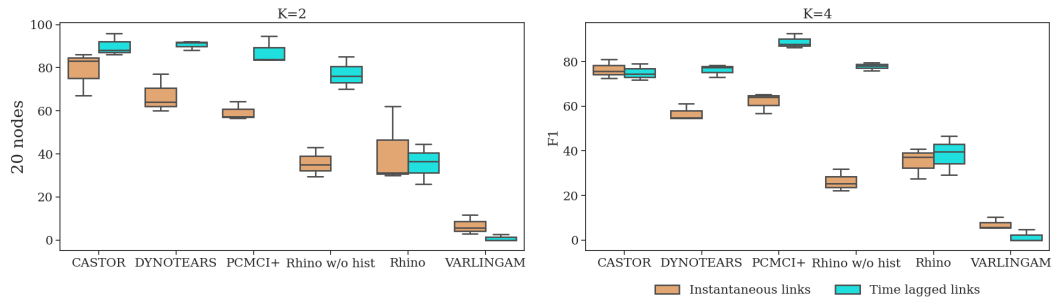


Figure 10: F1 scores by Models and Settings: Orange indicates performance on instantaneous links, and sky-blue signifies performance on time-lagged relationships. Notably, **CASTOR is the only model capable of learning the number of regimes and regime indices; for other baselines, a manual split was performed beforehand.** Number of nodes is 20 nodes

In this section, we present also some additional results using non-linear synthetic data with varying numbers of nodes, specifically $\{10, 20\}$, and diverse numbers of regimes $\{2, 3, 4\}$. In this case, we compare our model against various baseline models, namely DYNOTEARS [27], Rhino [12], PCMCI+ [34] and VARLINGAM [18]. For setting with 10 nodes, we can see from Figure (10) that CASTOR, Rhino, PCMCI+ and DYNOTEARS exhibit superior performance to VARLINGAM. It is important to outline that Rhino, PCMCI+, DYNOTEARS and VARLINGAM are each applied to individual regimes separately; neither is designed to learn or infer the number or indices of regimes. PCMCI+ outperforms CASTOR, Rhino and DYNOTEARS in modeling time-lagged relations for non-linear scenarios. PCMCI+ demonstrates robustness in capturing non-linear relationships. Benefiting from a manual split performed beforehand, PCMCI+ exhibits comparable performance (for $K = 2$) or outperforms (for $K = 4$) CASTOR in capturing time-lagged relations. These results are understandable due to the fact that CASTOR has to learn more aspects, including the number of regimes and their indices. For instantaneous links, CASTOR consistently outperforms all models. In the case of $K = 3$ regimes, CASTOR outperforms all models in instantaneous links and achieves comparable results in time-lagged relations as DYNOTEARS and PCMCI+. Notably, Rhino, a state-of-the-art causal discovery model, exhibits lower performance than DYNOTEARS and PCMCI+, consistent with the findings reported by Rhino authors in their appendix when testing Rhino in settings with non historical dependent noise. Moreover, Rhino requires a substantial amount of

data for training (50 MTS with 200 time steps), while our setting only includes regimes with 600 time steps.

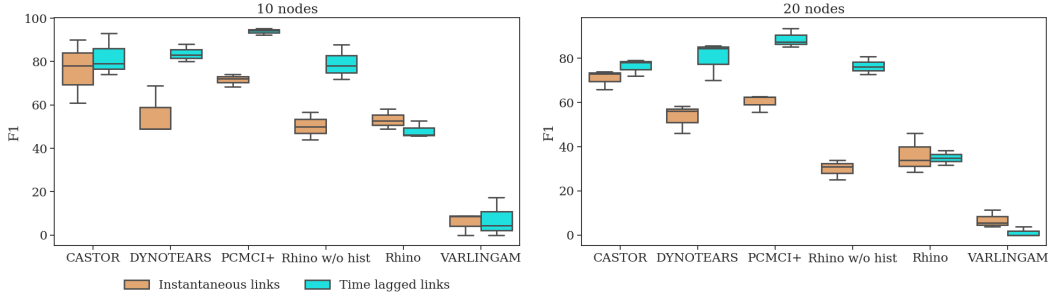


Figure 11: F1 by Models for $K=3$ Setting: Gray indicates performance on instantaneous links, and pink signifies performance on time-lagged relationships. Notably, **CASTOR is the only model capable of learning the number of regimes and regime indices; for other baselines, a manual split was performed beforehand.**

E.6 Further experiments: Comparison with CD-NOD

We conducted a comparative analysis with CD-NOD, a causal discovery model specifically designed for heterogeneous data and non-stationary time series [16]. In the context of MTS with multiple regimes, CD-NOD learns a summary causal graph encapsulating the entire MTS.

It’s worth noting that in the work by [16], CD-NOD demonstrates the capability to learn both the change points and the summary causal graph. We use the open-source code of CD-NOD implemented in Matlab by the authors⁷.

Our experimental setup involves linear causal relations and diverse configurations, including 2, 3, and 4 regimes, each with varying numbers of nodes (10, 20, 40). For independence test of CD-NOD, we chose Fisher’s Z conditional independence test for linear causal relationships and KCI independent test for non linear relations. We systematically compared the performance of CD-NOD against CASTOR, with the evaluation centered on the summary causal graphs as the basis for comparison.

Definition E.1. (Summary causal graph, [3]) Let $(x_t)_{t \in \mathcal{T}}$ be a MTS and $\mathcal{G} = (V, E)$ the associated summary causal graph. The set of vertices in that graph consists of the set of components x^1, \dots, x^d at each time $t \in \mathbb{N}$. The edges E of the graph are defined as follows: variables x^p and x^q are connected if and only if there exists some time t and some time lag τ such that $x_{t-\tau}^p$ causes x_t^q at time t with a time lag of $0 \leq \tau$ for $p \neq q$ and with a time lag of $0 < \tau$ for $p = q$.

d	Method	$K = 2$	$K = 3$	$K = 4$
10	CD-NOD	20.2	11.4	38.8
	CASTOR	100	100	97.9
20	CD-NOD	25.2	23.7	12.7
	CASTOR	100	97.2	93.4
40	CD-NOD	0	11.3	5.57
	CASTOR	100	99.8	99.2

Table 5: F1 Scores by Models and Settings: d indicates number of nodes and K refers to the number of regimes. The comparison is made for linear relations.

From Table 5, we can notice that CD-NOD does not manage to outperform CASTOR in various settings (with an F1 score that does not exceed 26%). Additionally, a clear trend emerges where

⁷<https://github.com/Biwei-Huang/Causal-Discovery-from-Nonstationary-Heterogeneous-Data>

CD-NOD’s performance declines when the number of nodes is 40. On the contrary, CASTOR exhibits consistent performance across different settings, achieving a F1 score of over 93% in all scenarios.

	$d = 10$	
	$K = 2$	$K = 3$
CD-NOD	28.5	25.3
CASTOR	86.1	85.2

Table 6: F1 Scores by Models and Settings: d indicates number of nodes and K refers to the number of regimes. The comparison is made for non linear relations.

From Table 6, CD-NOD with KCI independent does not manage to outperform CASTOR in non linear causal relationships settings (with an F1 score that does not exceed 28%). This is understandable, because firstly, CD-NOD learns one summary graph. The model assumes smooth changes in graphs between regimes i.e. it expects only a few variables of the graph to be affected by the regime switch (Assumption may not hold true in scenarios such as epileptic seizures or climate science). However, CASTOR did not have this assumption and also learn one causal graph per regime.

E.7 Further experiments: Regime detection experiment

We compare CASTOR to CD-NOD [16] and KCP [2] in the task of regime detection. KCP is a multiple change-point detection method designed to handle univariate, multivariate, or complex data. Being non-parametric, KCP does not necessitate knowing the true number of change points in advance. It detects abrupt changes in the complete distribution of the data by employing a characteristic kernel.

As we described in the previous section, CD-NOD is a causal discovery model specifically designed for heterogeneous data and non-stationary time series. In phase III of CD-NOD, a method is proposed to learn change points (that occur when causal relationships changes) for MTS with multiple regimes. CD-NOD estimates a non-stationary driving force for each component (node, considering its parents), where this driving force is a function of the time index. If the driving force changes with the time index, it indicates a change in the regime for that component; otherwise, it signifies that the component is within the same regime.

As previously explained, CD-NOD learns a driving force for components that change behavior. To detect the regimes, one approach is to learn the change points for all components exhibiting changing behavior and then form the union of these change points, yielding the regime partition.

In contrast to CD-NOD, CASTOR directly learns the regime indices. Consequently, for every sample, CASTOR assigns it to a specific regime, directly yielding the regime partition. Additionally, CASTOR conducts regime detection at the graph level rather than the node level which makes it faster than CD-NOD in the task of regime detection.

We opted to perform regime detection in two settings: one with 10 nodes and four different regimes, and another with 20 nodes and four distinct regimes, the causal relationships are non linear in this scenario. For a fair comparison, we chose four regimes without re-occurrence, as KCP and CD-NOD only detect change points and cannot identify the re-occurrence of a specific regime. CASTOR excels in this regard since it detects regime indices. For instance, if regime u occurs from $t = 1$ to $t = 400$ and then reoccurs from $t = 1000$ to $t = 1300$, CASTOR encompasses all these indices in the previously defined regime partition \mathcal{E}_u . It utilizes all these indices collectively to learn a more accurate graph.

Regarding the models employed, we use the open-source code of CD-NOD implemented in Matlab by the authors⁸. For KCP, we employ the Rupture package⁹.

⁸<https://github.com/Biwei-Huang/Causal-Discovery-from-Nonstationary-Heterogeneous-Data>

⁹<https://centre-borelli.github.io/ruptures-docs/>

	Regime accuracy $K = 4$ and $d = 10$	Regime accuracy $K = 4$ and $d = 20$
KCP	33.4	66.8
CD-NOD	70.1	88.2
CASTOR	95.9	98.7

Table 7: Regime detection accuracy by models: CASTOR and CD-NOD outperform the state-of-the-art change-point detection method KCP. CASTOR achieves maximum accuracy, surpassing 95% for both settings.

From the table, it is evident that causal models (CASTOR and CD-NOD) outperform the change-point detection method KCP. This outcome can be attributed to the limitation of KCP in detecting changing points within causal mechanisms that are represented by conditional distributions. CASTOR outperforms CD-NOD in detecting regime indices. This result can be explained by the fact that CASTOR learns regime indices based on graph-level change points, while CD-NOD detects change points at the node level. The node-level approach in CD-NOD may not effectively detect simultaneous changes in behavior for components that actually change behavior simultaneously.

From this analysis, we can conclude that in scenarios involving MTS with multiple regimes and unknown regime indices, CASTOR offers a robust solution. Additionally, employing other methods to split the regimes and learn the causal graph through traditional causal discovery methods may not be an optimal solution:

- We demonstrate that regime indices are not well recoverable by CD-NOD and other state-of-the-art change point detection method KCP. Therefore, employing CD-NOD or KCP to learn the regimes and subsequently using methods like DYNOTEARS, PCMCI, or Rhino to learn the graph may not constitute an optimal solution.
- In cases of regime recurrence, the aforementioned methods are unable to accurately detect the exact number of regimes. Therefore, if a user employs CD-NOD and subsequently uses the regime partitions revealed by CD-NOD as an input to a causal discovery method (such as PCMCI+, DYNOTEARS, Rhino, etc.), the running time will be significantly high.

Example: To elaborate further, let’s consider the epilepsy setting. Imagine we have a recording from an epileptic patient where the sequence involves a non-seizure phase, followed by a seizure phase, and then a reappearance of the non-seizure phase. Employing CD-NOD, particularly with a KCI independence test, to detect regimes in such a scenario can be computationally expensive (For the table above scenario with 20 nodes CD-NOD takes more than 24h compared to CASTOR that learns the regimes and the graph in less than 1h). Subsequently, applying algorithms like Rhino, DYNOTEARS, or Lingam to learn temporal causal graphs would also be resource-intensive. This is primarily because the user would need to run the chosen algorithm at least three times (twice for non-seizure and once for seizure) since CD-NOD does not clarify that a the non-seizure regime is reappearing.

E.8 Models running time

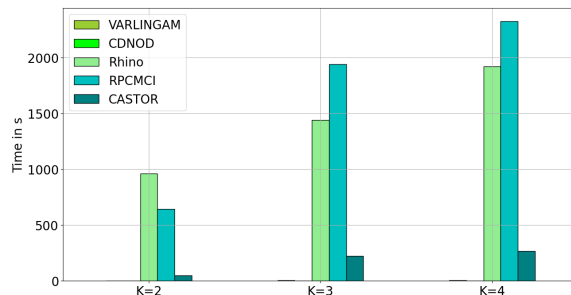


Figure 12: Running time per model, the y axis represents the running time in s and the x axis the number of regime

We compute the running time of every model in different settings, that includes 10 nodes and 2,3 or 4 different regimes, Figure 12 summarizes the results.

VARLINGAM and CD-NOD (employing Fisher's Z conditional independence test for faster runs; note that KCI CD-NOD takes over 2000 seconds for 2 regimes, and more than 24h for scenario with 4 regimes and 20 nodes as mentioned in the previous section) exhibit remarkable speed compared to other methods. However, in terms of scores, both models encounter challenges in effectively learning causal graphs. Notably, CASTOR runs faster than Rhino, even though CASTOR learns both temporal causal graphs and regime indices.

A fair comparison arises when comparing RPCMCI and CASTOR, as both models learn regime indices and temporal causal graphs. It's essential to mention that RPCMCI necessitates specifying the number of regimes and the maximum number of transitions, producing only time-lagged relations. From Figure 12, it is apparent that CASTOR converges more rapidly than RPCMCI. This difference in convergence time becomes more pronounced as the settings become more complex.

F Regime and causal graphs identifiability

In this section, we concentrate on establishing the identifiability of regimes and causal graphs within the CASTOR framework. Before diving into the details, let us set and clarify the required assumptions.

Definition F.1. (Causal Stationarity [33]). The time series (that has one regime) process $(\mathbf{x}_t)_{t \in \mathcal{T}}$ with a graph \mathcal{G} is called causally stationary over a time index set \mathcal{T} if and only if for all links $x_{t-\tau}^i \rightarrow x_t^j$ in the graph

$$x_{t-\tau}^i \not\perp\!\!\!\perp x_t^j \mid \mathbf{x}_{<t} \setminus \{x_{t-\tau}^i\} \text{ holds for all } t \in \mathcal{T}$$

This elucidates the inherent characteristics of the time-series data generation mechanism, thereby validating the choice of the auto-regressive model. In our setting, we generalize Causal Stationarity as follows:

Assumption F.2. (Causal Stationarity for time series with multiple regimes). The time series process $(\mathbf{x}_t)_{t \in \mathcal{T}}$ comprise multiple regimes K , where K is the number of regime, we note $\mathcal{E}_u = \{t \mid \gamma_{t,u} = 1\}$ the set of time indices where the regime u is active, and $\mathcal{T} = \cup_u \mathcal{E}_u$. $(\mathbf{x}_t)_{t \in \mathcal{T}}$ with a graph $\{\mathcal{G}^u\}_{u \in \{1, \dots, K\}}$ is called causally stationary over a time index set \mathcal{T} if and only if for all $u \in \{1, \dots, K\}$, $(\mathbf{x}_t)_{t \in \mathcal{E}_u}$ is causal stationary with graph \mathcal{G}^u for time index set \mathcal{E}_u .

Definition F.3. (Causal Markov Property, [31]). Given a DAG \mathcal{G} and a joint distribution p , this distribution is said to satisfy causal Markov property w.r.t. the DAG \mathcal{G} if each variable is independent of its non-descendants given its parents.

This is a common assumptions for the distribution induced by an SEM. With this assumption, one can deduce conditional independence between variables from the graph.

Assumption F.4. (Causal Markov Property for multiple regimes). Given a set of DAGs $(\mathcal{G}^u)_{u \in \{1, \dots, K\}}$ and a set of joint distribution $(p(\cdot \mid \mathcal{G}^u))_{u \in \{1, \dots, K\}}$, we say that this set of distributions satisfies causal Markov property w.r.t. the set of DAGs $(\mathcal{G}^u)_{u \in \{1, \dots, K\}}$ if for every u : $p(\cdot \mid \mathcal{G}^u)$ satisfy causal Markov property w.r.t the DAG \mathcal{G}^u .

Definition F.5. (Causal Minimality, [12]). Consider a distribution p and a DAG \mathcal{G} , we say this distribution satisfies causal minimality w.r.t. \mathcal{G} if it is Markovian w.r.t. \mathcal{G} but not to any proper subgraph of \mathcal{G} .

Assumption F.6. (Causal Minimality for multiple regimes). Given a set of DAGs $(\mathcal{G}^u)_{u \in \{1, \dots, K\}}$ and a set of joint distribution $(p(\cdot \mid \mathcal{G}^u))_{u \in \{1, \dots, K\}}$, we say that this set of distributions satisfies causal minimality w.r.t. the set of DAGs $(\mathcal{G}^u)_{u \in \{1, \dots, K\}}$ if for every u : $p(\cdot \mid \mathcal{G}^u)$ satisfy causal minimality w.r.t the DAG \mathcal{G}^u .

Assumption F.7. (Causal Sufficiency). A set of observed variables V is causally sufficient for a process \mathbf{x}_t if and only if in the process every common cause of any two or more variables in V is in V or has the same value for all units in the population.

This assumption implies there are no latent confounders present in the time-series data.

Assumption F.8. (Well-defined Density). We assume the joint likelihood induced by the CASTOR SEM (Eq. (1)) is absolutely continuous w.r.t. a Lebesgue or counting measure and $\forall u : |\log p(\mathbf{x}_{t \in \mathcal{E}_u}; \mathcal{G}^u)| < \infty$ for all possible \mathcal{G}^u .

This presumption ensures that the resulting distribution possesses a well-defined probability density function. It is also necessary for Markov factorization property.

Assumption F.9. (CASTOR in DAG space). We assume the CASTOR framework can only return the solutions from DAG space.

The table 8 illustrates that most assumptions (causal sufficiency, causal Markov, DAGness, well-defined density, faithfulness/minimality) are commonly shared among various state-of-the-art models in causal discovery.

However, CASTOR, RPCMCI, and CD-NOD relax the assumption of stationarity and instead assume that the MTS (Multivariate Time Series) are composed of different regimes. While CD-NOD predicts

Table 8: Summary of the main assumptions of algorithms considered in the paper. For causal graphs, S means that the algorithm provides a summary causal graph and W means that the algorithm provides a window causal graph; F corresponds to faithfulness and M to minimality. An empty cell mean that the information given in the corresponding column was not discussed by the authors of the corresponding algorithm.

	Causal graph	Causal Markov	Causal sufficiency	Faithfulness / Minimality	Linear model	Stationarity MTS composed of one regime	Stationarity per regime	Well defined density	Dagness Space
DYNOTEARS	W	✓	✓		✓	✓			✓
PCMCI+	W	✓	✓	F	×	✓		✓	✓
RPCMCI	W	✓	✓	F	×	×	✓	✓	✓
Rhino	W	✓	✓	M	×	✓		✓	✓
VARLINGAM	W	✓	✓		✓	✓			✓
CD-NOD	S	✓	✓	F	×	×	✓	✓	✓
CASTOR	W	✓	✓	M	×	×	✓	✓	✓

only a summary causal graph, CASTOR and RPCMCI predict a window causal graph, which can subsequently be used to reconstruct a summary graph.

One notable difference in assumptions between CASTOR and RPCMCI is that RPCMCI assumes only time-lagged relations, whereas CASTOR incorporates the presence of instantaneous links.

F.1 Proof of theorem 1

Assuming the aforementioned assumptions we want to prove the theorem 4.1.

We consider $\mathcal{G} = (\mathcal{G}^u)_{u \in \{1, \dots, N_w\}}$, $\mathcal{E} = \cup_{u=1}^{N_w} \mathcal{E}_u$ where N_w is the number of window, $\mathcal{G}^* = (\mathcal{G}^{*,u})_{u \in \{1, \dots, K\}}$, K is the exact number of true regimes and $\mathcal{E}^* = \cup_{u=1}^K \mathcal{E}_u^*$. We denote $\mathcal{E}_c \mathcal{E}_\ell^*$ the set of time indices that is shared between regime c of our model estimation and the true regime ℓ and $q_\ell^* := \frac{|\mathcal{E}_\ell^*|}{T}$, $q_c := \frac{|\mathcal{E}_c|}{T}$, $q_{c\ell} := \frac{|\mathcal{E}_c \mathcal{E}_\ell^*|}{T}$. Our objective is to prove that for any estimation $(\hat{\mathcal{G}}, \hat{\mathcal{E}})$: if $\exists u \in \{1, \dots, K\}$ s.t. $\hat{\mathcal{G}}^u$ disagree with $\mathcal{G}^{*,u}$ on instantaneous or/and time lagged link, or any regime $\hat{\mathcal{E}}_u \in \hat{\mathcal{E}}$ is close to none of the true regimes in the sense of Kullback–Leibler divergence: $\mathcal{S}(\mathcal{G}^*, \mathcal{E}^*) > \mathcal{S}(\hat{\mathcal{G}}, \hat{\mathcal{E}})$. We have by Eq (7):

$$\mathcal{S}(\mathcal{G}, \mathcal{E}) := \sup_{\theta, \mathcal{G}} \frac{1}{T} \sum_{u=1}^{N_u} \sum_{t \in \mathcal{E}_u} \log f^u(\mathbf{x}_t) - \lambda |\mathcal{G}^u|,$$

where λ is the sparsity penalty coefficient and $f^u(\mathbf{x}_t) := \prod_{j=1}^d f_j^u(\mathbf{Pa}_{\mathcal{G}^u}^i(< t), \mathbf{Pa}_{\mathcal{G}^u}^i(t))$ with $f_j^u(\mathbf{Pa}_{\mathcal{G}^u}^i(< t), \mathbf{Pa}_{\mathcal{G}^u}^i(t))$ the function used to describe the distribution family in Eq (5). We will structure the proof as follows:

- Prove that if the score is optimized, then all the estimated regimes will be pure (have only elements of the same true regime).
- Prove that, when the regimes are pure and $N_w = K$, we have $\mathcal{S}(\mathcal{G}^*, \mathcal{E}^*) > \mathcal{S}(\hat{\mathcal{G}}, \hat{\mathcal{E}})$ for any estimation $\hat{\mathcal{G}}$ where $\exists u \in \{1, \dots, K\}$ s.t. $\hat{\mathcal{G}}^u$ disagrees with $\mathcal{G}^{*,u}$ on instantaneous or/and time lagged link.

F.1.1 Optimizing the score will lead to pure regimes

We denote by $p^{(u)}$ the distribution $p(\cdot | \mathcal{G}^u)$, ignoring penalty terms, we have:

$$\begin{aligned}
-\mathcal{S}(\mathcal{G}, \mathcal{E}) &= -\sup_{\theta} \sum_{c=1}^{N_w} \sum_{\ell=1}^K q_{c\ell} \frac{1}{|\mathcal{E}_c \mathcal{E}_{\ell}^*|} \sum_{t \in \mathcal{E}_c \mathcal{E}_{\ell}^*} [\log f^c(\mathbf{x}_t)] \\
&\rightarrow -\sup_{\phi} \sum_{c=1}^{N_w} \sum_{\ell=1}^K q_{c\ell} \mathbb{E}_{\mathbf{x}_t \sim p^{(\ell)}} [\log f^c] \\
&= -\sup_{\theta} \sum_{c=1}^{N_w} \sum_{\ell=1}^K q_{c\ell} \mathbb{E}_{\mathbf{x}_t \sim p^{(\ell)}} \left[\sum_{i=1}^d \log f_i^c(\mathbf{Pa}_{\mathcal{G}^c}^i(< t), \mathbf{Pa}_{\mathcal{G}^c}^i(t)) \right] \\
&= -\sup_{\theta} \sum_{c=1}^{N_w} \sum_{\ell=1}^K \sum_{i=1}^d q_{c\ell} \\
&\quad \mathbb{E}_{\mathbf{x}_t \sim p^{(\ell)}} \left[-\log \frac{p(x_t^i | (\mathbf{Pa}_{\mathcal{G}^{*,\ell}}^i(< t), \mathbf{Pa}_{\mathcal{G}^{*,\ell}}^i(t)))}{f_i^c(\mathbf{Pa}_{\mathcal{G}^c}^i(< t), \mathbf{Pa}_{\mathcal{G}^c}^i(t))} + \log p(x_t^i | (\mathbf{Pa}_{\mathcal{G}^{*,\ell}}^i(< t), \mathbf{Pa}_{\mathcal{G}^{*,\ell}}^i(t))) \right] \\
&= -\sup_{\theta} \sum_{c=1}^{N_w} \sum_{\ell=1}^K \sum_{i=1}^d q_{c\ell} \\
&\quad \mathbb{E}_{\mathbf{x}_t \sim p^{(\ell)}} \left[-\text{D}_{\text{KL}}(p(x_t^i | (\mathbf{Pa}_{\mathcal{G}^{*,\ell}}^i(< t), \mathbf{Pa}_{\mathcal{G}^{*,\ell}}^i(t))) \| f_i^c(\mathbf{Pa}_{\mathcal{G}^c}^i(< t), \mathbf{Pa}_{\mathcal{G}^c}^i(t))) \right. \\
&\quad \left. - \text{H}(p(x_t^i | (\mathbf{Pa}_{\mathcal{G}^{*,\ell}}^i(< t), \mathbf{Pa}_{\mathcal{G}^{*,\ell}}^i(t)))) \right] \\
&= -\sup_{\theta} \sum_{c=1}^{N_w} \sum_{\ell=1}^K \sum_{i=1}^d q_{c\ell} \mathbb{E}_{\mathbf{x}_t \sim p^{(\ell)}} [-\text{D}_{\text{KL}}(p(x_t^i | (\mathbf{Pa}_{\mathcal{G}^{*,\ell}}^i(< t), \mathbf{Pa}_{\mathcal{G}^{*,\ell}}^i(t))) \| f_i^c(\mathbf{Pa}_{\mathcal{G}^c}^i(< t), \mathbf{Pa}_{\mathcal{G}^c}^i(t)))] \\
&\quad - \sup_{\theta} \sum_{c=1}^{N_c} \sum_{\ell=1}^K \sum_{i=1}^d q_{c\ell} \mathbb{E}_{\mathbf{x}_t \sim p^{(\ell)}} [-\text{H}(p(x_t^i | (\mathbf{Pa}_{\mathcal{G}^{*,\ell}}^i(< t), \mathbf{Pa}_{\mathcal{G}^{*,\ell}}^i(t)))] \\
&= \inf_{\theta} \sum_{c=1}^{N_w} \sum_{\ell=1}^K \sum_{j=1}^d q_{c\ell} \mathbb{E}_{\mathbf{x}_t \sim p^{(\ell)}} [\text{D}_{\text{KL}}(p(x_t^i | (\mathbf{Pa}_{\mathcal{G}^{*,\ell}}^i(< t), \mathbf{Pa}_{\mathcal{G}^{*,\ell}}^i(t))) \| f_i^c(\mathbf{Pa}_{\mathcal{G}^c}^i(< t), \mathbf{Pa}_{\mathcal{G}^c}^i(t)))] \\
&\quad + \sum_{c=1}^{N_w} \sum_{\ell=1}^K \sum_{j=1}^d q_{c\ell} \mathbb{E}_{\mathbf{x}_t \sim p^{(\ell)}} [\text{H}(p(x_t^i | (\mathbf{Pa}_{\mathcal{G}^{*,\ell}}^i(< t), \mathbf{Pa}_{\mathcal{G}^{*,\ell}}^i(t)))] \\
&= \inf_{\theta} \sum_{c=1}^{N_w} \sum_{\ell=1}^K \sum_{i=1}^d q_{c\ell} \mathbb{E}_{\mathbf{x}_t \sim p^{(\ell)}} [\text{D}_{\text{KL}}(p(x_t^i | (\mathbf{Pa}_{\mathcal{G}^{*,\ell}}^i(< t), \mathbf{Pa}_{\mathcal{G}^{*,\ell}}^i(t))) \| f_i^c(\mathbf{Pa}_{\mathcal{G}^c}^i(< t), \mathbf{Pa}_{\mathcal{G}^c}^i(t)))] \\
&\quad + \sum_{\ell=1}^K \sum_{i=1}^d \left(\sum_{c=1}^{N_c} q_{c\ell} \right) \mathbb{E}_{\mathbf{x}_t \sim p^{(\ell)}} [\text{H}(p(x_t^i | (\mathbf{Pa}_{\mathcal{G}^{*,\ell}}^i(< t), \mathbf{Pa}_{\mathcal{G}^{*,\ell}}^i(t)))] \\
&= \inf_{\theta} \sum_{c=1}^{N_w} \sum_{\ell=1}^K \sum_{i=1}^d q_{c\ell} \mathbb{E}_{\mathbf{x}_t \sim p^{(\ell)}} [\text{D}_{\text{KL}}(p(x_t^i | (\mathbf{Pa}_{\mathcal{G}^{*,\ell}}^i(< t), \mathbf{Pa}_{\mathcal{G}^{*,\ell}}^i(t))) \| f_i^c(\mathbf{Pa}_{\mathcal{G}^c}^i(< t), \mathbf{Pa}_{\mathcal{G}^c}^i(t)))] \\
&\quad + \sum_{\ell=1}^K \sum_{i=1}^d q_{\ell}^* \mathbb{E}_{\mathbf{x}_t \sim p^{(\ell)}} [\text{H}(p(x_t^i | (\mathbf{Pa}_{\mathcal{G}^{*,\ell}}^i(< t), \mathbf{Pa}_{\mathcal{G}^{*,\ell}}^i(t)))]
\end{aligned} \tag{5}$$

Note that θ could be the parameters of the neural networks used in Eq (3.4) for non linear causal relationship or $\theta = (\mathcal{G}^u)_{u \in \{1, \dots, N_w\}}$ for linear case Eq 8.

For the score of ground truth (ignoring penalty terms):

$$-\mathcal{S}(\mathcal{G}^*, \mathcal{E}^*) \rightarrow 0 + \sum_{\ell=1}^K \sum_{i=1}^d q_{\ell}^* \mathbb{E}_{\mathbf{x}_t \sim p^{(\ell)}} [\mathbb{H}(p(x_t^i | (\mathbf{Pa}_{\mathcal{G}^*, \ell}^i(< t), \mathbf{Pa}_{\mathcal{G}^*, \ell}^i(t))))] \quad (\text{by Assumption 5 F.8}) \quad (6)$$

Combining Equation (5) and Equation (6), we have (considering penalty terms):

$$\begin{aligned} \mathcal{S}(\mathcal{G}^*, \mathcal{E}^*) - \mathcal{S}(\mathcal{G}, \mathcal{E}) &= \inf_{\theta} \sum_{c=1}^{N_w} \sum_{\ell=1}^K \sum_{i=1}^d q_{c\ell} \\ &\quad \mathbb{E}_{\mathbf{x}_t \sim p^{(\ell)}} [\text{D}_{\text{KL}}(p(x_t^i | (\mathbf{Pa}_{\mathcal{G}^*, \ell}^i(< t), \mathbf{Pa}_{\mathcal{G}^*, \ell}^i(t)))) \| f_i^c(\mathbf{Pa}_{\mathcal{G}^c}^i(< t), \mathbf{Pa}_{\mathcal{G}^c}^i(t)))] \\ &\quad + \lambda \left(\sum_{c=1}^{N_w} |\mathcal{G}^c| - \sum_{\ell=1}^K |\mathcal{G}^{*, \ell}| \right) \end{aligned} \quad (7)$$

The first term in Equation (7) is the score term, others are penalty term.

In the following lines, our goal is to demonstrate that optimizing the score term ensures that all identified regimes will accurately match the real regimes. In other words, each estimated regime will be a true representation of an actual one. Additionally, by shifting samples from less significant regimes (regimes with few samples) to the most similar significant regimes, our variable N_w will eventually stabilize at the value of K . To do this, we will proceed by contradiction:

Suppose the score term in Eq (7) is optimized and there exists a regime e that is **not pure**, i.e., there exist $a, b \in [K]$ with $a \neq b$ but $q_{ea} > 0$ and $q_{eb} > 0$. Since they are different distributions for two different regimes with two different causal graphs, there exists $i \in \{1, \dots, d\}$ such that $p(x_t^i | (\mathbf{Pa}_{\mathcal{G}^*, a}^i(< t), \mathbf{Pa}_{\mathcal{G}^*, a}^i(t))) \neq p(x_t^i | (\mathbf{Pa}_{\mathcal{G}^*, b}^i(< t), \mathbf{Pa}_{\mathcal{G}^*, b}^i(t)))$. Then the score term in Equation (7) has the following lower bound:

$$\begin{aligned} &\inf_{\theta} \sum_{\ell=1}^K \sum_{i=1}^d q_{e\ell} \mathbb{E}_{\mathbf{x}_t \sim p^{(\ell)}} [\text{D}_{\text{KL}}(p(x_t^i | (\mathbf{Pa}_{\mathcal{G}^*, \ell}^i(< t), \mathbf{Pa}_{\mathcal{G}^*, \ell}^i(t)))) \| f_i^e(\mathbf{Pa}_{\mathcal{G}^e}^i(< t), \mathbf{Pa}_{\mathcal{G}^e}^i(t)))] \\ &\geq \inf_{\theta} \left\{ q_{ea} \mathbb{E}_{\mathbf{x}_t \sim p^{(a)}} [\text{D}_{\text{KL}}(p(x_t^i | (\mathbf{Pa}_{\mathcal{G}^*, a}^i(< t), \mathbf{Pa}_{\mathcal{G}^*, a}^i(t)))) \| f_i^e(\mathbf{Pa}_{\mathcal{G}^e}^i(< t), \mathbf{Pa}_{\mathcal{G}^e}^i(t)))] \right. \\ &\quad \left. + q_{eb} \mathbb{E}_{\mathbf{x}_t \sim p^{(b)}} [\text{D}_{\text{KL}}(p(x_t^i | (\mathbf{Pa}_{\mathcal{G}^*, b}^i(< t), \mathbf{Pa}_{\mathcal{G}^*, b}^i(t)))) \| f_i^e(\mathbf{Pa}_{\mathcal{G}^e}^i(< t), \mathbf{Pa}_{\mathcal{G}^e}^i(t)))] \right\} \end{aligned} \quad (8)$$

As we assumed that the score term in Eq (7) is optimized, it means that:

$$\begin{aligned} 0 &= \inf_{\theta} \sum_{c=1}^{N_w} \sum_{\ell=1}^K \sum_{i=1}^d q_{c\ell} \mathbb{E}_{\mathbf{x}_t \sim p^{(\ell)}} [\text{D}_{\text{KL}}(p(x_t^i | (\mathbf{Pa}_{\mathcal{G}^*, \ell}^i(< t), \mathbf{Pa}_{\mathcal{G}^*, \ell}^i(t)))) \| f_i^c(\mathbf{Pa}_{\mathcal{G}^c}^i(< t), \mathbf{Pa}_{\mathcal{G}^c}^i(t)))] \\ &\Rightarrow 0 = \inf_{\theta} \sum_{\ell=1}^K \sum_{i=1}^d q_{e\ell} \mathbb{E}_{\mathbf{x}_t \sim p^{(\ell)}} [\text{D}_{\text{KL}}(p(x_t^i | (\mathbf{Pa}_{\mathcal{G}^*, \ell}^i(< t), \mathbf{Pa}_{\mathcal{G}^*, \ell}^i(t)))) \| f_i^e(\mathbf{Pa}_{\mathcal{G}^e}^i(< t), \mathbf{Pa}_{\mathcal{G}^e}^i(t)))] \\ &\Rightarrow \begin{cases} \text{D}_{\text{KL}}(p(x_t^i | (\mathbf{Pa}_{\mathcal{G}^*, a}^i(< t), \mathbf{Pa}_{\mathcal{G}^*, a}^i(t)))) \| f_i^e(\mathbf{Pa}_{\mathcal{G}^e}^i(< t), \mathbf{Pa}_{\mathcal{G}^e}^i(t)) = 0 \\ \text{D}_{\text{KL}}(p(x_t^i | (\mathbf{Pa}_{\mathcal{G}^*, b}^i(< t), \mathbf{Pa}_{\mathcal{G}^*, b}^i(t)))) \| f_i^e(\mathbf{Pa}_{\mathcal{G}^e}^i(< t), \mathbf{Pa}_{\mathcal{G}^e}^i(t)) = 0 \end{cases} \\ &\Rightarrow \forall i \in \{1, \dots, d\} : p(x_t^i | (\mathbf{Pa}_{\mathcal{G}^*, a}^i(< t), \mathbf{Pa}_{\mathcal{G}^*, a}^i(t))) = p(x_t^i | (\mathbf{Pa}_{\mathcal{G}^*, b}^i(< t), \mathbf{Pa}_{\mathcal{G}^*, b}^i(t))) \end{aligned} \quad (9)$$

and the last line, Eq (9), is a contradiction because the two distributions represent two different regimes with two different graphs. Hence, if the score term of Eq (7) is optimized all the estimated regimes will be pure.

First case: If we matched the samples of less significant regimes to the wrong regimes, the regime is not pure and then the score term is not optimized (contradiction).

Second case: If we eliminate a lot of regimes such that $N_w \leq K - 1$, at least one of our estimated regimes will not be pure and this contradicts the assumption of optimized score term (same reasoning).

Based on this reasoning, optimizing the score term of Equation (7) will ensure convergence to the true number of regimes and also every regime will be pure.

F.1.2 In case of edge disagreement $\mathcal{S}(\mathcal{G}^*, \mathcal{E}^*) > \mathcal{S}(\hat{\mathcal{G}}, \hat{\mathcal{E}})$

Now we will show that Eq (7) is positive, if $\exists u \in \{1, \dots, K\}$ s.t $\hat{\mathcal{G}}^u$ disagrees with $\mathcal{G}^{*,u}$ on instantaneous or/and time lagged link.

To simplify the notation, we denote by $p^{(u)}$ the distribution $p(\cdot | \mathcal{G}^u)$ the optimal distribution that describes the CGM of regime u . We assume that each estimated regime $\hat{\mathcal{E}}_c$ ($c \in \{1, \dots, N_w\}$, $N_w \geq K$) contains samples from same true regime. Then Equation (7) has lower bound:

$$\begin{aligned} & \inf_{\theta} \sum_{\ell=1}^K q_{\ell}^* \mathbb{E}_{\mathbf{x}_t \sim p^{(\ell)}} \text{D}_{\text{KL}}(p^{(\ell)} \| f^{\ell}) \\ & \geq (\min_{\ell} q_{\ell}^*) \inf_{\theta} \sum_{\ell=1}^K \text{D}_{\text{KL}}(p^{(\ell)} \| f^{\ell}) \end{aligned} \quad (10)$$

Equation (10) is positive if and only if $\eta(\mathcal{G})$ is positive.

$$\eta(\mathcal{G}) := \inf_{\theta} \sum_{\ell=1}^K \text{D}_{\text{KL}}(p^{(\ell)} \| f^{\ell}) \quad (11)$$

Let assume that $\exists r \in \{1, \dots, K\}$ s.t $\hat{\mathcal{G}}^r$ disagrees with $\mathcal{G}^{*,r}$ on instantaneous or/and time lagged link. We follow the same intuition as [12, 30, 31], we will show that $\text{D}_{\text{KL}}(p^{(r)} \| f^r)$ is positive in two cases:

- **Disagreement on lagged parents only.** This means that for all $t \in [\mathcal{S} + 1, T]$, the instantaneous connections at t for $\hat{\mathcal{G}}^r$ and $\mathcal{G}^{*,r}$ are the same, and $\exists t \in [\mathcal{S} + 1, T]$ and $i \in \{1, \dots, d\}$ such that $\mathbf{Pa}_{\hat{\mathcal{G}}^r}^{x_t^i}(< t) \neq \overline{\mathbf{Pa}}_{\mathcal{G}^{*,r}}^{x_t^i}(< t)$. We can use a similar argument as the theorem 1 in [30]. Without loss of generality, we assume under $\hat{\mathcal{G}}^r$, we have $x_{t-\tau}^j \rightarrow x_t^i$ and there is no connections between them under $\mathcal{G}^{*,r}$. Thus, from Markov conditions, we have

$$x_t^i \perp\!\!\!\perp x_{t-\tau}^j \mid \mathbf{Pa}_{\hat{\mathcal{G}}^r}^{x_t^i}(< t) \cup \text{ND}_t^{x_t^i} \setminus \{x_t^i, x_{t-\tau}^j\}$$

under $\mathcal{G}^{*,r}$, where $\text{ND}_t^{x_t^i}$ are the non-descendants of node x_t^i at some time t . However, from the causal minimality and Proposition 6.16 in [31], we have

$$x_t^i \not\perp\!\!\!\perp x_{t-\tau}^j \mid \overline{\mathbf{Pa}}_{\mathcal{G}^{*,r}}^{x_t^i}(< t) \cup \text{ND}_t^{x_t^i} \setminus \{x_t^i, x_{t-\tau}^j\}$$

under $\hat{\mathcal{G}}^r$, and we have $\text{D}_{\text{KL}}(p^{(r)} \| f^r) \neq 0$

- **Disagreement on instantaneous parents.** In this Section we will use two different results one for the linear and the other one for the non linear case.
 - *Linear case.* For this case, we will use Theorem 1 in [28]. In this theorem, the author confirms that the graph is identifiable for linear models with Gaussian additive noise, if for each $j \in \{1, \dots, d\}$, the weights of the causal relations $\beta_{jk} \neq 0$ for all $k \in \mathbf{Pa}_j^{\mathcal{G}^0}$. For our instantaneous links, we have all the weights of the parents are non null. Hence, the instantaneous links are identifiable. Otherwise if $\text{D}_{\text{KL}}(p^{(r)} \| f^r) \neq 0$
 - *Non linear case.* Using Theorem 2 from [29], we can notice that our instantaneous links are Identifiable Functional Model Class, $(\mathcal{B}, \mathcal{F})$ -IFMOC, they belongs exactly to the 3rd class of Lemma 3 in [29]: nonlinear ANMs: $\mathcal{F}_3 = \{f(X, n) = \phi(X) + n\}$ $\mathcal{B}_3 = \{(\phi, X, N) \text{ not lin., Gauss, Gauss}\} \setminus \tilde{\mathcal{B}}_3$. Hence our instantaneous links are identifiable, otherwise, $\text{D}_{\text{KL}}(p^{(r)} \| f^r) \neq 0$.

Based on the above reasoning, we can show that if $\exists r \in \{1, \dots, K\}$ s.t., $\hat{\mathcal{G}}^r$ disagree with $\mathcal{G}^{*,r}$ on instantaneous or/and time lagged links, $D_{\text{KL}}(p^{(r)} \| f^r) \neq 0$.

Thus, $\eta(\mathcal{G}) > 0$. Then as we assume in Theorem 4.1 that λ is sufficient small would implies Equation (9) is positive.

If $|\hat{\mathcal{G}}^r| \geq |\mathcal{G}^{*,r}|$ then clearly Eq 9 is positive. Let $\mathbb{G}^+ := \left\{ \hat{\mathcal{G}}^r \in \mathbb{G} \mid |\hat{\mathcal{G}}^r| < |\mathcal{G}^{*,r}| \right\}$. To make sure that we have $\mathcal{S}(\mathcal{G}^*, \mathcal{E}^*) - \mathcal{S}(\mathcal{G}, \mathcal{E}) > 0$ for all $\mathcal{G} \in \mathbb{G}^+$, we need to pick λ sufficiently small. Choosing $0 < \lambda < \min_{\mathcal{G} \in \mathbb{G}^+} \frac{\eta(\mathcal{G})}{(\sum_{c=1}^{N_w} |\mathcal{G}^c| - \sum_{\ell=1}^K |\mathcal{G}^{*,\ell}|)}$ is sufficient.

F.2 Proof of theorem 4.2

Our objective is to prove that for any estimations $(\mathcal{G}, \mathcal{E})$ and $(\mathcal{G}', \mathcal{E}')$ such that $(\mathcal{G}, \mathcal{E})$ is closer in terms of Kullback–Leibler to the optimal solution $(\mathcal{G}^*, \mathcal{E}^*)$ than $(\mathcal{G}', \mathcal{E}')$: $\mathcal{S}(\mathcal{G}, \mathcal{E}) > \mathcal{S}(\mathcal{G}', \mathcal{E}')$. Our goal is to demonstrate that, for any estimation $(\mathcal{G}, \mathcal{E})$, one that is closer in terms of Kullback-Leibler (KL) divergence to the optimal solution $(\mathcal{G}^*, \mathcal{E}^*)$ will have a higher score estimated by CASTOR compared to another estimation $(\mathcal{G}', \mathcal{E}')$. To clarify, when we mention "closer to $(\mathcal{G}^*, \mathcal{E}^*)$ in terms of KL," we are referring to the degree of similarity to the optimal solution $(\mathcal{G}^*, \mathcal{E}^*)$. In other terms for every regime ℓ :

$$\begin{aligned} & D_{\text{KL}}(p(x_t^i \mid (\mathbf{Pa}_{\mathcal{G}^{*,\ell}}^i(<t), \mathbf{Pa}_{\mathcal{G}^{*,\ell}}^i(t)))) \| f_i^\ell(\mathbf{Pa}_{\mathcal{G}^\ell}^i(<t), \mathbf{Pa}_{\mathcal{G}^\ell}^i(t))) \\ & \leq D_{\text{KL}}(p(x_t^i \mid (\mathbf{Pa}_{\mathcal{G}^{*,\ell}}^i(<t), \mathbf{Pa}_{\mathcal{G}^{*,\ell}}^i(t)))) \| f_i^\ell(\mathbf{Pa}_{\mathcal{G}'^\ell}^i(<t), \mathbf{Pa}_{\mathcal{G}'^\ell}^i(t))) \end{aligned} \quad (12)$$

First case: Let's assume, in this first scenario, that both suboptimal estimations $((\mathcal{G}', \mathcal{E}^*)$ and $(\mathcal{G}, \mathcal{E}^*))$ accurately detect the regimes, with the only distinction lying in the estimation of the graph.

We know that the score function of each estimation after the optimization procedure could be written as the following:

$$\begin{aligned} -\mathcal{S}(\mathcal{G}, \mathcal{E}^*) &= \sum_{\ell=1}^K \sum_{i=1}^d q_\ell^* \mathbb{E}_{\mathbf{x}_t \sim p^{(\ell)}} [D_{\text{KL}}(p(x_t^i \mid (\mathbf{Pa}_{\mathcal{G}^{*,\ell}}^i(<t), \mathbf{Pa}_{\mathcal{G}^{*,\ell}}^i(t)))) \| f_i^\ell(\mathbf{Pa}_{\mathcal{G}^\ell}^i(<t), \mathbf{Pa}_{\mathcal{G}^\ell}^i(t)))] \\ &+ \sum_{\ell=1}^K \sum_{i=1}^d q_\ell^* \mathbb{E}_{\mathbf{x}_t \sim p^{(\ell)}} [H(p(x_t^i \mid (\mathbf{Pa}_{\mathcal{G}^{*,\ell}}^i(<t), \mathbf{Pa}_{\mathcal{G}^{*,\ell}}^i(t))))] \\ -\mathcal{S}(\mathcal{G}', \mathcal{E}^*) &= \sum_{\ell=1}^K \sum_{i=1}^d q_\ell^* \mathbb{E}_{\mathbf{x}_t \sim p^{(\ell)}} [D_{\text{KL}}(p(x_t^i \mid (\mathbf{Pa}_{\mathcal{G}^{*,\ell}}^i(<t), \mathbf{Pa}_{\mathcal{G}^{*,\ell}}^i(t)))) \| f_i^\ell(\mathbf{Pa}_{\mathcal{G}'^\ell}^i(<t), \mathbf{Pa}_{\mathcal{G}'^\ell}^i(t)))] \\ &+ \sum_{\ell=1}^K \sum_{i=1}^d q_\ell^* \mathbb{E}_{\mathbf{x}_t \sim p^{(\ell)}} [H(p(x_t^i \mid (\mathbf{Pa}_{\mathcal{G}^{*,\ell}}^i(<t), \mathbf{Pa}_{\mathcal{G}^{*,\ell}}^i(t))))] \\ \mathcal{S}(\mathcal{G}, \mathcal{E}^*) - \mathcal{S}(\mathcal{G}', \mathcal{E}^*) &= \sum_{\ell=1}^K \sum_{i=1}^d q_\ell^* \mathbb{E}_{\mathbf{x}_t \sim p^{(\ell)}} [D_{\text{KL}}(p(x_t^i \mid (\mathbf{Pa}_{\mathcal{G}^{*,\ell}}^i(<t), \mathbf{Pa}_{\mathcal{G}^{*,\ell}}^i(t)))) \| f_i^\ell(\mathbf{Pa}_{\mathcal{G}'^\ell}^i(<t), \mathbf{Pa}_{\mathcal{G}'^\ell}^i(t)))] \\ &- D_{\text{KL}}(p(x_t^i \mid (\mathbf{Pa}_{\mathcal{G}^{*,\ell}}^i(<t), \mathbf{Pa}_{\mathcal{G}^{*,\ell}}^i(t)))) \| f_i^\ell(\mathbf{Pa}_{\mathcal{G}^\ell}^i(<t), \mathbf{Pa}_{\mathcal{G}^\ell}^i(t)))] \\ \mathcal{S}(\mathcal{G}, \mathcal{E}^*) - \mathcal{S}(\mathcal{G}', \mathcal{E}^*) &\geq 0 \end{aligned} \quad (13)$$

In the first case, we demonstrated that if two estimations differ in the graph learning component, the one closer to the optimal solution will have a higher score. The last inequality is correct even when we add the sparsity term because, we can pick λ sufficiently small, to ensure that we have $\mathcal{S}(\mathcal{G}, \mathcal{E}^*) - \mathcal{S}(\mathcal{G}', \mathcal{E}^*) > 0$.

Second case: Let's assume that both suboptimal estimations $((\mathcal{G}, \mathcal{E}')$ and $(\mathcal{G}, \mathcal{E}))$ learn identical causal graphs for all regimes. However, for the estimation \mathcal{E}' , there exists at least one regime a that misclassifies more S samples and incorrectly assigns them to regime b .

We know that the score function of each estimation after the optimization procedure could be written as the following:

$$\begin{aligned}
-\mathcal{S}(\mathcal{G}, \mathcal{E}) &= \sum_{c=1}^{N_w} \sum_{\ell=1}^K \sum_{i=1}^d q_{c\ell} \mathbb{E}_{\mathbf{x}_t \sim p^{(\ell)}} [D_{\text{KL}}(p(x_t^i | (\mathbf{Pa}_{\mathcal{G}^*, \ell}^i(< t), \mathbf{Pa}_{\mathcal{G}^*, \ell}^i(t))) \| f_i^c(\mathbf{Pa}_{\mathcal{G}^c}^i(< t), \mathbf{Pa}_{\mathcal{G}^c}^i(t)))] \\
&\quad + \sum_{\ell=1}^K \sum_{i=1}^d q_{\ell}^* \mathbb{E}_{\mathbf{x}_t \sim p^{(\ell)}} [\text{H}(p(x_t^i | (\mathbf{Pa}_{\mathcal{G}^*, \ell}^i(< t), \mathbf{Pa}_{\mathcal{G}^*, \ell}^i(t)))] \\
-\mathcal{S}(\mathcal{G}', \mathcal{E}') &= \sum_{c=1}^{N_w} \sum_{\ell=1}^K \sum_{i=1}^d q'_{c\ell} \mathbb{E}_{\mathbf{x}_t \sim p^{(\ell)}} [D_{\text{KL}}(p(x_t^i | (\mathbf{Pa}_{\mathcal{G}^*, \ell}^i(< t), \mathbf{Pa}_{\mathcal{G}^*, \ell}^i(t))) \| f_i^c(\mathbf{Pa}_{\mathcal{G}^c}^i(< t), \mathbf{Pa}_{\mathcal{G}^c}^i(t)))] \\
&\quad + \sum_{\ell=1}^K \sum_{i=1}^d q_{\ell}^* \mathbb{E}_{\mathbf{x}_t \sim p^{(\ell)}} [\text{H}(p(x_t^i | (\mathbf{Pa}_{\mathcal{G}^*, \ell}^i(< t), \mathbf{Pa}_{\mathcal{G}^*, \ell}^i(t)))]
\end{aligned} \tag{14}$$

As previously explained, for the estimation \mathcal{E}' , S samples from regime a are misclassified as belonging to regime b . This implies: $q'_{aa} = q_{aa} - \frac{S}{|\mathcal{T}|}$ and $q'_{ba} = q_{ba} + \frac{S}{|\mathcal{T}|}$, and we have the difference between the 2 scores is written as follows:

$$\begin{aligned}
\mathcal{S}(\mathcal{G}, \mathcal{E}) - \mathcal{S}(\mathcal{G}', \mathcal{E}') &= \sum_{i=1}^d \frac{S}{|\mathcal{T}|} \mathbb{E}_{\mathbf{x}_t \sim p^{(a)}} [D_{\text{KL}}(p(x_t^i | (\mathbf{Pa}_{\mathcal{G}^*, a}^i(< t), \mathbf{Pa}_{\mathcal{G}^*, a}^i(t))) \| f_i^b(\mathbf{Pa}_{\mathcal{G}^b}^i(< t), \mathbf{Pa}_{\mathcal{G}^b}^i(t))) \\
&\quad - D_{\text{KL}}(p(x_t^i | (\mathbf{Pa}_{\mathcal{G}^*, a}^i(< t), \mathbf{Pa}_{\mathcal{G}^*, a}^i(t))) \| f_i^a(\mathbf{Pa}_{\mathcal{G}^a}^i(< t), \mathbf{Pa}_{\mathcal{G}^a}^i(t)))] \\
\mathcal{S}(\mathcal{G}, \mathcal{E}^*) - \mathcal{S}(\mathcal{G}', \mathcal{E}^*) &\geq 0
\end{aligned} \tag{15}$$

The aforementioned equation is positive because, by definition, the distribution estimated by CASTOR for regime a is closer to the true distribution of regime b than the estimation of the distribution for regime b .

Third case: Let's assume that there exists at least one regime a that misclassifies more samples S and incorrectly assigns them to regime b . In these two regimes, the two suboptimal estimations yield different causal graphs. However, as previously described, the regime indices learned by \mathcal{E} are closer to \mathcal{E}^* . In other words, \mathcal{E}' misclassifies more samples S from regime a and incorrectly assigns them to regime b . Additionally, the graph inferred by \mathcal{G} is closer to the optimal solution than the graph \mathcal{G}' estimated by the second suboptimal method.

We assume that $q_{ba} \ll q_{aa}$, signifying that the number of well-classified regime samples is greater than the number of misclassified samples. This assumption is reasonable because altering graphs between regimes will cause changes in the mean of our mixtures f^u . Furthermore, given the higher dimension, making slight modifications such as deleting a few edges and adding new ones will result in distinct mixtures. Consequently, the number of samples that could be misclassified will be low.

We know that the score function of each estimation after the optimization procedure could be written as the following:

$$\begin{aligned}
-\mathcal{S}(\mathcal{G}, \mathcal{E}) &= \sum_{c=1}^{N_w} \sum_{\ell=1}^K \sum_{i=1}^d q_{c\ell} \mathbb{E}_{\mathbf{x}_t \sim p^{(\ell)}} [D_{\text{KL}}(p(x_t^i | (\mathbf{Pa}_{\mathcal{G}^*, \ell}^i(< t), \mathbf{Pa}_{\mathcal{G}^*, \ell}^i(t))) \| f_i^c(\mathbf{Pa}_{\mathcal{G}^c}^i(< t), \mathbf{Pa}_{\mathcal{G}^c}^i(t)))] \\
&\quad + \sum_{\ell=1}^K \sum_{i=1}^d q_{\ell}^* \mathbb{E}_{\mathbf{x}_t \sim p^{(\ell)}} [\text{H}(p(x_t^i | (\mathbf{Pa}_{\mathcal{G}^*, \ell}^i(< t), \mathbf{Pa}_{\mathcal{G}^*, \ell}^i(t)))]
\end{aligned} \tag{16}$$

$$\begin{aligned}
-\mathcal{S}(\mathcal{G}', \mathcal{E}') &= \sum_{c=1}^{N_w} \sum_{\ell=1}^K \sum_{i=1}^d q'_{c\ell} \mathbb{E}_{\mathbf{x}_t \sim p^{(\ell)}} [D_{\text{KL}}(p(x_t^i | (\mathbf{Pa}_{\mathcal{G}^*, \ell}^i(< t), \mathbf{Pa}_{\mathcal{G}^*, \ell}^i(t))) \| f_i^c(\mathbf{Pa}_{\mathcal{G}'c}^i(< t), \mathbf{Pa}_{\mathcal{G}'c}^i(t)))] \\
&\quad + \sum_{\ell=1}^K \sum_{i=1}^d q_{\ell}^* \mathbb{E}_{\mathbf{x}_t \sim p^{(\ell)}} [H(p(x_t^i | (\mathbf{Pa}_{\mathcal{G}^*, \ell}^i(< t), \mathbf{Pa}_{\mathcal{G}^*, \ell}^i(t)))] \\
\mathcal{S}(\mathcal{G}, \mathcal{E}) - \mathcal{S}(\mathcal{G}', \mathcal{E}') &= \sum_{i=1}^d \frac{S}{|\mathcal{T}|} \mathbb{E}_{\mathbf{x}_t \sim p^{(a)}} [D_{\text{KL}}(p(x_t^i | (\mathbf{Pa}_{\mathcal{G}^*, a}^i(< t), \mathbf{Pa}_{\mathcal{G}^*, a}^i(t))) \| f_i^b(\mathbf{Pa}_{\mathcal{G}'b}^i(< t), \mathbf{Pa}_{\mathcal{G}'b}^i(t)))] \\
&\quad - D_{\text{KL}}(p(x_t^i | (\mathbf{Pa}_{\mathcal{G}^*, a}^i(< t), \mathbf{Pa}_{\mathcal{G}^*, a}^i(t))) \| f_i^a(\mathbf{Pa}_{\mathcal{G}'a}^i(< t), \mathbf{Pa}_{\mathcal{G}'a}^i(t))) \\
&\quad + \sum_{i=1}^d q_{aa} \mathbb{E}_{\mathbf{x}_t \sim p^{(a)}} [D_{\text{KL}}(p(x_t^i | (\mathbf{Pa}_{\mathcal{G}^*, a}^i(< t), \mathbf{Pa}_{\mathcal{G}^*, a}^i(t))) \| f_i^a(\mathbf{Pa}_{\mathcal{G}'a}^i(< t), \mathbf{Pa}_{\mathcal{G}'a}^i(t)))] \\
&\quad - D_{\text{KL}}(p(x_t^i | (\mathbf{Pa}_{\mathcal{G}^*, a}^i(< t), \mathbf{Pa}_{\mathcal{G}^*, a}^i(t))) \| f_i^a(\mathbf{Pa}_{\mathcal{G}^a}^i(< t), \mathbf{Pa}_{\mathcal{G}^a}^i(t))) \\
&\quad + \sum_{i=1}^d q_{ba} \mathbb{E}_{\mathbf{x}_t \sim p^{(a)}} [D_{\text{KL}}(p(x_t^i | (\mathbf{Pa}_{\mathcal{G}^*, a}^i(< t), \mathbf{Pa}_{\mathcal{G}^*, a}^i(t))) \| f_i^b(\mathbf{Pa}_{\mathcal{G}'b}^i(< t), \mathbf{Pa}_{\mathcal{G}'b}^i(t)))] \\
&\quad - D_{\text{KL}}(p(x_t^i | (\mathbf{Pa}_{\mathcal{G}^*, a}^i(< t), \mathbf{Pa}_{\mathcal{G}^*, a}^i(t))) \| f_i^b(\mathbf{Pa}_{\mathcal{G}^b}^i(< t), \mathbf{Pa}_{\mathcal{G}^b}^i(t))) \\
\mathcal{S}(\mathcal{G}, \mathcal{E}) - \mathcal{S}(\mathcal{G}', \mathcal{E}') &\approx \sum_{i=1}^d \frac{S}{|\mathcal{T}|} \mathbb{E}_{\mathbf{x}_t \sim p^{(a)}} [D_{\text{KL}}(p(x_t^i | (\mathbf{Pa}_{\mathcal{G}^*, a}^i(< t), \mathbf{Pa}_{\mathcal{G}^*, a}^i(t))) \| f_i^b(\mathbf{Pa}_{\mathcal{G}'b}^i(< t), \mathbf{Pa}_{\mathcal{G}'b}^i(t)))] \\
&\quad - D_{\text{KL}}(p(x_t^i | (\mathbf{Pa}_{\mathcal{G}^*, a}^i(< t), \mathbf{Pa}_{\mathcal{G}^*, a}^i(t))) \| f_i^a(\mathbf{Pa}_{\mathcal{G}'a}^i(< t), \mathbf{Pa}_{\mathcal{G}'a}^i(t))) \\
&\quad + \sum_{i=1}^d q_{aa} \mathbb{E}_{\mathbf{x}_t \sim p^{(a)}} [D_{\text{KL}}(p(x_t^i | (\mathbf{Pa}_{\mathcal{G}^*, a}^i(< t), \mathbf{Pa}_{\mathcal{G}^*, a}^i(t))) \| f_i^a(\mathbf{Pa}_{\mathcal{G}'a}^i(< t), \mathbf{Pa}_{\mathcal{G}'a}^i(t)))] \\
&\quad - D_{\text{KL}}(p(x_t^i | (\mathbf{Pa}_{\mathcal{G}^*, a}^i(< t), \mathbf{Pa}_{\mathcal{G}^*, a}^i(t))) \| f_i^a(\mathbf{Pa}_{\mathcal{G}^a}^i(< t), \mathbf{Pa}_{\mathcal{G}^a}^i(t))) \\
\mathcal{S}(\mathcal{G}, \mathcal{E}^*) - \mathcal{S}(\mathcal{G}', \mathcal{E}^*) &\geq 0
\end{aligned} \tag{17}$$

The last inequality is correct for these two last cases, even when we add the sparsity term because, we can pick λ sufficiently small, to ensure that we have $\mathcal{S}(\mathcal{G}, \mathcal{E}) - \mathcal{S}(\mathcal{G}', \mathcal{E}') > 0$.

G Illustration of CASTOR's estimated graphs

G.1 Illustration of the estimated graphs by CASTOR: Linear case, 5 regimes with $L = 1$



Figure 13: The estimated temporal causal graphs for five regimes (**Linear case**) consist of one matrix of 10 rows and 10 columns representing instantaneous links and another of 10 rows and 10 columns delineating time-lagged relations (with a maximum lag $L = 1$ in this case). Dark blue indicates a value of one (presence of an edge), while sky blue symbolizes a value of 0 (absence of an edge). The second column displays the groundtruth causal graphs, and the final column highlights the difference between the estimated and true graphs.

G.2 Illustration of the estimated graphs by CASTOR: Linear case, 2 regimes with $L = 2$

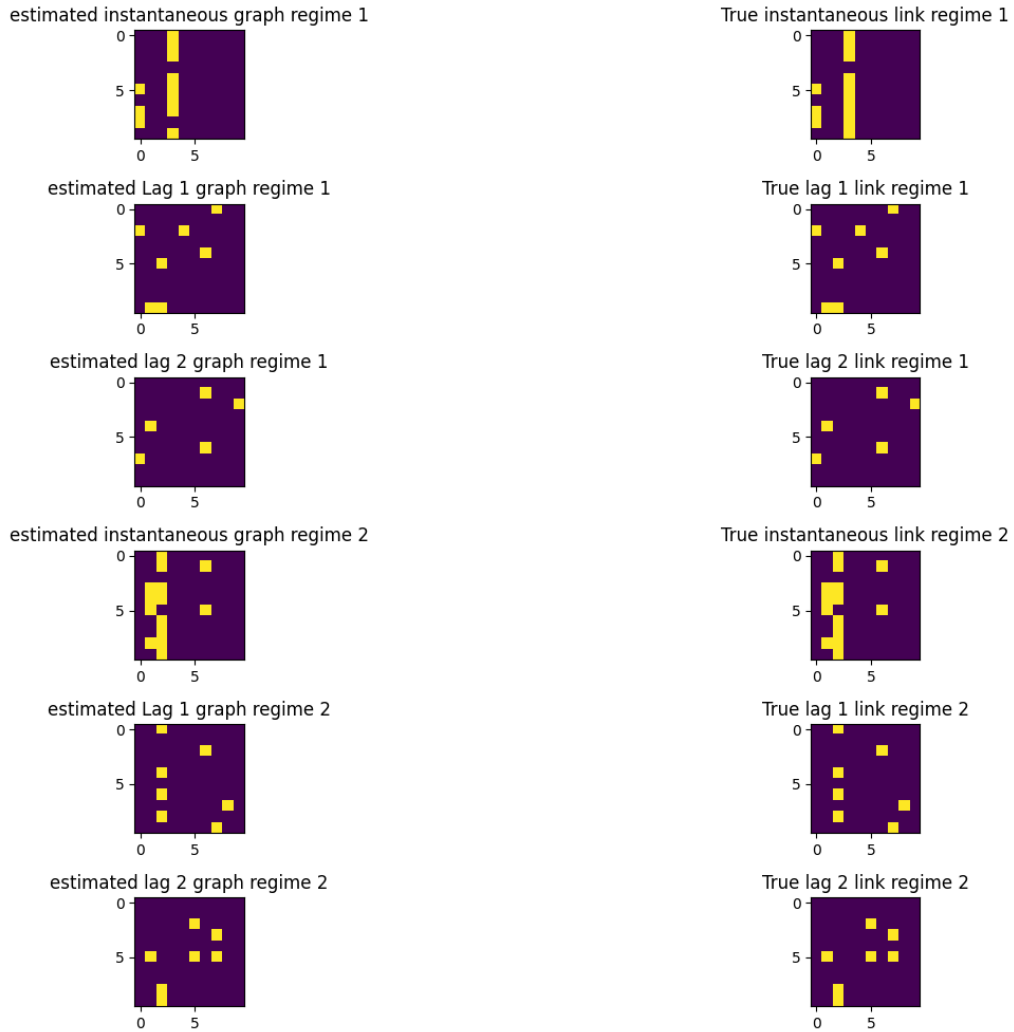


Figure 14: The estimated temporal causal graphs for two regimes (**non Linear case**), with one matrix representing instantaneous links and another delineating time-lagged relations. The second column showcases the actual causal graphs, while the final column highlights the discrepancies between the estimated and true graphs. Yellow indicates a value of one (presence of an edge), while black symbolizes a value of 0 (absence of an edge).

G.3 Illustration of the estimated graphs by CASTOR: Non-linear case, 3 regimes with $L = 1$

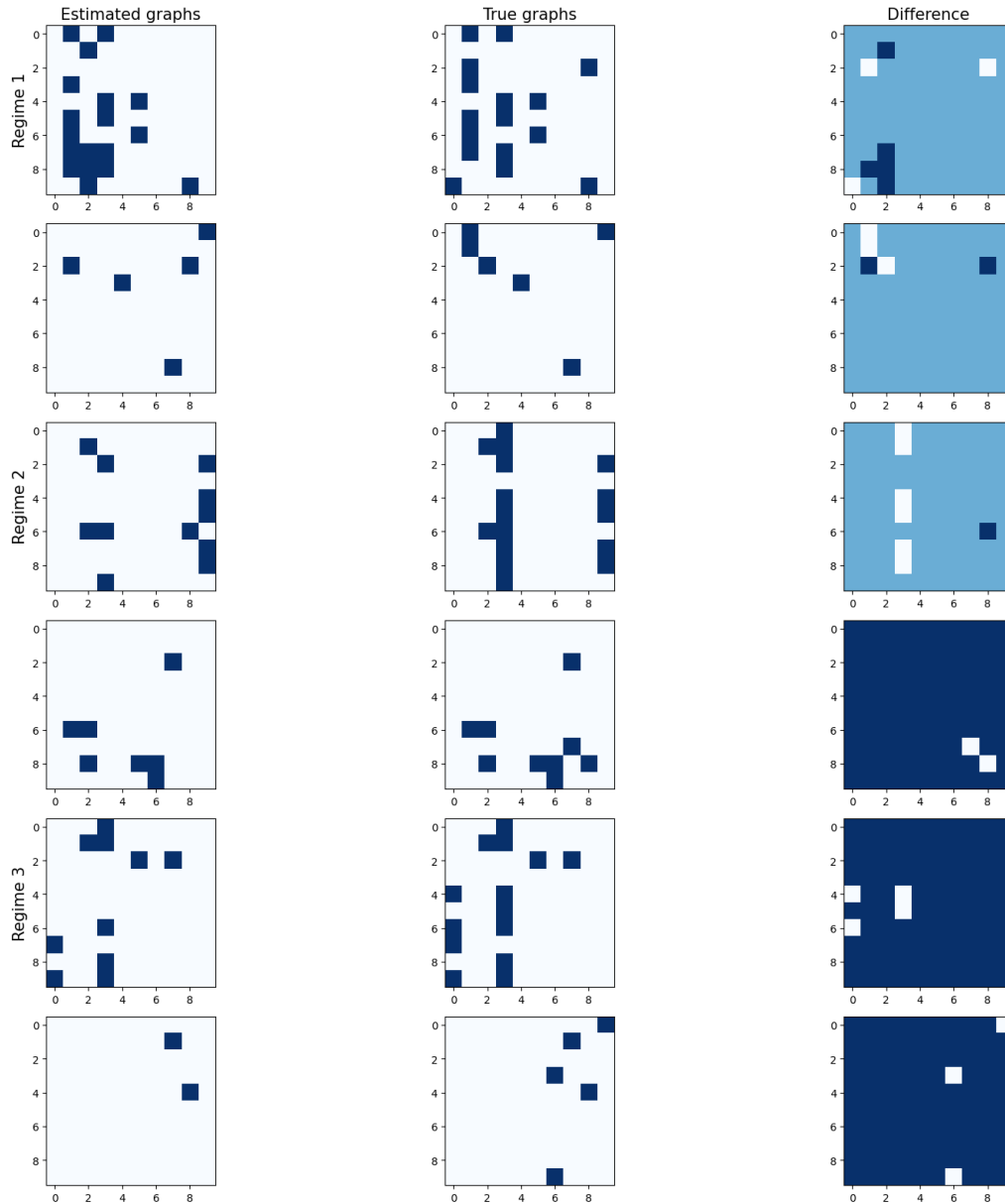


Figure 15: The estimated temporal causal graphs for three regimes (**Non-Linear case**) consist of one matrix of 10 rows and 10 columns representing instantaneous links and another of 10 rows and 10 columns delineating time-lagged relations (with a maximum lag $L = 1$ in this case). Dark blue indicates a value of one (presence of an edge), while sky blue symbolizes a value of 0 (absence of an edge). The second column displays the groundtruth causal graphs, and the final column highlights the difference between the estimated and true graphs.

G.4 Illustration of the estimated graphs by CASTOR: Non-linear case, 5 regimes with $L = 1$

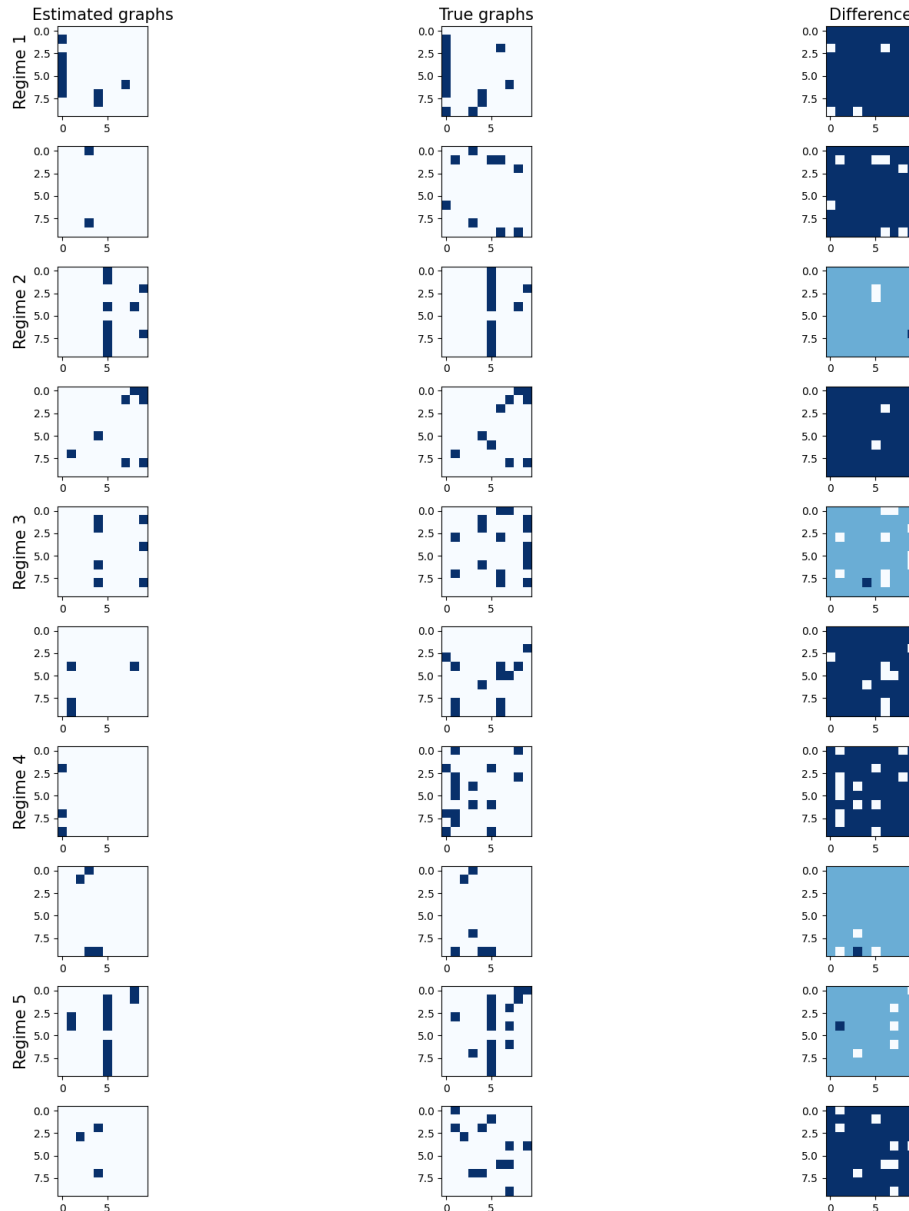


Figure 16: The estimated temporal causal graphs for five regimes (**Non-Linear case**) consist of one matrix of 10 rows and 10 columns representing instantaneous links and another of 10 rows and 10 columns delineating time-lagged relations (with a maximum lag $L = 1$ in this case). Dark blue indicates a value of one (presence of an edge), while sky blue symbolizes a value of 0 (absence of an edge). The second column displays the groundtruth causal graphs, and the final column highlights the difference between the estimated and true graphs.